

Broadband Extended Array Response-Based Subspace Multiparameter Estimation Method for Multipolarized Wireless Channel Measurements

Bensheng Yang^{ID}, *Graduate Student Member, IEEE*, Peize Zhang^{ID}, *Graduate Student Member, IEEE*, Haiming Wang^{ID}, *Member, IEEE*, Cheng-Xiang Wang^{ID}, *Fellow, IEEE*, and Xiaohu You^{ID}, *Fellow, IEEE*

Abstract—The clustered delay line channel model, in which each cluster consists of many rays, is widely used for link-level evaluations in mobile communications. Multiple parameters of each ray, including the delay, amplitude, cross-polarization ratio (XPR), initial phases of four polarization combinations, and the azimuth and elevation angles of arrival and departure, must be known and are measured using a channel sounder. The number of rays in every cluster is usually greater than the number of elements in the antenna array of the channel sounder, which represents a challenging issue in multipolarized channel measurements. Based on the broadband extended array response of an electromagnetic vector antenna array, a new subspace estimation method is proposed to resolve a large number of rays. The inter-element spacing of the array can be greater than half the carrier wavelength, which reduces inter-element coupling and simplifies the array design, especially for millimeter-wave bands. The delay of each cluster is first estimated using the reference antenna element. Next, two-dimensional angles of every ray are estimated using the classic rank-deficient multiple signal classification algorithm. Finally, the initial phases, XPR, and amplitude of every ray are estimated. Simulation results validate the proposed method.

Index Terms—Broadband extended array response (BEAR), channel measurements, cross-polarization ratio (XPR), electromagnetic vector antenna array (EMVAA), subspace estimation method.

I. INTRODUCTION

THE performance of wireless transmission in mobile communication systems is directly dependent on the channel

Manuscript received June 10, 2020; revised October 29, 2020 and December 21, 2020; accepted February 2, 2021. Date of publication February 10, 2021; date of current version May 18, 2021. This work was supported in part by the National Key R&D Program of China under Grant 2020YFB1804901, the National Natural Science Foundation of China under Grant 61960206006, and the Key R&D Program of Jiangsu Province of China under Grant BE2018121. The associate editor coordinating the review of this article and approving it for publication was Y. Li. (*Corresponding author: Haiming Wang.*)

Bensheng Yang, Peize Zhang, and Haiming Wang are with the State Key Laboratory of Millimeter Waves, Southeast University, Nanjing 210096, China, and also with Purple Mountain Laboratories, Nanjing 211111, China (e-mail: yangbensheng@seu.edu.cn; pzzhang@seu.edu.cn; hmwang@seu.edu.cn).

Cheng-Xiang Wang and Xiaohu You are with the National Mobile Communications Research Laboratory, Southeast University, Nanjing 210096, China, and also with Purple Mountain Laboratories, Nanjing 211111, China (e-mail: chxwang@seu.edu.cn; xhyu@seu.edu.cn).

Color versions of one or more figures in this article are available at <https://doi.org/10.1109/TCOMM.2021.3058372>.

Digital Object Identifier 10.1109/TCOMM.2021.3058372

propagation characteristics. Therefore, a multiparameter estimation method for in-depth analysis of channel propagation characteristics and channel modeling of the mobile communication systems is important [1], [2]. In the study item for channel models in the 3rd Generation Partnership Project (3GPP), delay, two-dimensional (2D) ¹ angles of departure (AoD), 2D angles of arrival (AoA), and cross-polarization ratio (XPR) are essential small-scale parameters [3]–[5]. An accurate and efficient multiparameter estimation method is of great significance in channel measurements. Moreover, ray polarization must be considered in channel modeling. Antenna polarization modeling is also advocated by 3GPP.

Multipolarized multiple-input and multiple-output (MIMO) is a MIMO technique with transmit and receive arrays consisting of multipolarized antennas, e.g., tripolarized or hexapolarized antennas. A tripolarized antenna measures the electric field along three orthogonal directions. A hexapolarized antenna measures the electric field as well as the magnetic field along three orthogonal directions. Previous works have proved that multipolarized MIMO outperforms the corresponding unipolarized MIMO in terms of channel capacity in many situations [6]–[8]. Moreover, dual-polarized antenna configurations outperform single polarization in terms of spatial correlation [9]. The main reason for the capacity gain obtained by multipolarized MIMO relative to unipolarized MIMO is that the correlation between the antenna elements is reduced [10]. Due to these advantages, multipolarized MIMO is considered a promising technique for next-generation mobile communication systems. There has been increasing interest in polarized channel modeling and measurement, especially for multipolarized MIMO systems [10]–[13].

As a typical hexapolarized antenna, the electromagnetic vector antenna (EMVA) has been widely investigated in the literature on multipolarized array signal processing and capacity analysis [7], [14], [15]. However, due to the particularity of the EMVA structure, a collocated EMVA (C-EMVA) is complicated to construct [16]. The major difficulties originate from the antenna feeding method and the elimination of mutual coupling for the collocated elements. Such difficulties will be more apparent in the millimeter-wave multipolarized antenna design. To address these problems, a C-EMVA is

¹The two dimensions are the azimuth and elevation.

usually reconstructed as a non-collocated EMVA (NC-EMVA) or simplified to a dual- or triple-polarized antenna. The six polarization elements in NC-EMVA are no longer collocated but are placed separately in the form of an array [17], [18]. The NC-EMVA not only simplifies the EMVA design but also suppresses the mutual coupling between the antenna elements. The selection of the inter-element spacing (IES) of non-collocated antenna elements shall consider three aspects. The first one is mutual coupling suppression, which can be simulated by electromagnetic full-wave simulation software. The second one is the placement and heat dissipation of the radio frequency (RF) modules behind the array. The third one is the mobility of the channel sounding system for the practical channel measurement campaign.

Multiparameter estimation methods such as the maximum likelihood (ML) algorithm [19], multiple signal classification (MUSIC) [20], estimation of signal parameters via rotational invariance techniques (ESPRIT) and space-alternating generalized expectation-maximization (SAGE) [21], [22] have been investigated intensively in unipolarized array signal processing. In [21], [23], [24], the delay and AoA are estimated via a subspace-based method, and the number of total rays can be greater than the number of antenna elements but not the number of rays in one cluster.² In [22], [25], the delay, AoA, and fading coefficient are estimated using the SAGE algorithm. The SAGE and MUSIC algorithms are compared in [25] using measurement data. The multipolarized array signal processing algorithm has also received substantial attention, particularly for the EMVA [14], [15], [26]–[29].

However, a major difficulty in channel measurements is the parameter estimation of rays using multipolarized arrays when the number of rays in the cluster is greater than the number of array elements. The number of rays in one cluster often exceeds the number of antenna elements in the channel sounder [3], [4]. Existing multiparameter estimation methods usually do not work under such conditions or suffer from low robustness. Although the virtual MIMO can address this problem indirectly by shifting the antenna in space mechanically, it is inconvenient and leads to long measurement times. Therefore, an efficient method to overcome this difficulty with lower hardware complexity is needed.

In this study, a broadband extended array response (BEAR)-based subspace estimation method is proposed to address the issue of using the EMVA array (EMVAA). The dimension of the steering vector can be increased substantially via the BEAR. Traditionally, the AoA is obtained in the space domain, which requires the IES to be smaller than half the carrier wavelength. This requirement increases both the complexity of the channel sounding system and the mutual coupling between the antenna elements. The proposed method overcomes the limitation of IES, and the antenna array shape and IES are more flexible than in the traditional method. Furthermore, these advantages are more apparent in millimeter-wave MIMO

channel measurement systems. The main contributions of this work are summarized as follows.

- The BEAR-based subspace estimation method is proposed to estimate the delay, 2D AoD, 2D AoA, initial phases of the four polarization combination states, amplitude, and XPR in multipath environments using a multipolarized antenna array (EMVAA). In particular, the XPR of each ray is estimated in detail, rather than providing an approximate result with the power ratio of each polarized antenna element. Most of the parameters related to channel coefficient generation in the 3GPP protocol can be estimated.
- Using the proposed method, the RF module of the channel sounding system is simplified, and the mutual coupling in the antenna array is suppressed because the IES can be larger than half the carrier wavelength. Moreover, 2D angles can be estimated via linear EMVAA with low hardware complexity. Considering the complexity of the broadband loops in antenna design, the proposed method still works well with only dual- or triple-polarized antenna arrays.
- The number of rays in one cluster is greater than the number of antenna elements, which is a common difficulty in channel parameter estimation. The proposed BEAR-based method utilizes the response in the space-frequency-polarization (SFP) domain to solve this problem. The maximum number of rays that the proposed method can resolve is also given.

Notations: Upper (Lower) bold-face letters are used to denote matrices (vectors). A $K \times K$ identity matrix is denoted as \mathbf{I}_K . $\mathbf{1}_{M \times N}$ represents the $M \times N$ matrix with all elements equal to 1. The k th column vector of an identity matrix is a unit vector denoted as \mathbf{e}_k . Superscript $(\cdot)^H$ denotes the Hermitian transpose, and $(\cdot)^T$ denotes the transpose. The Hadamard product, Khatri-Rao product, and Kronecker product are, respectively, denoted by \odot , \oplus , and \otimes . A diagonal matrix with all entries of \mathbf{x} on the diagonal is denoted by $\text{diag}\{\mathbf{x}\}$. The phase angle of a complex number x is denoted by $\arg\{x\}$. The pseudoinverse of \mathbf{X} is represented as \mathbf{X}^\dagger . $\text{vec}\{\mathbf{X}\}$ represents the vectorization of \mathbf{X} .

II. SYSTEM MODEL

In this section, the clustered delay line (CDL) channel model, the multipolarized antenna system, and the received signal model are described. Subsequently, the SFP-domain channel response of the wireless channel measurement system is obtained. To clarify the system configuration, the parameters to be used in this work and the corresponding descriptions are listed in Table I.

A. Channel Model

In 3GPP, the CDL model is defined for the full frequency range from 0.5 GHz to 100 GHz, with a maximum bandwidth of 2 GHz, which is used mainly for link-level simulations [3]. In this channel model, the parameters that need to be estimated are the delays of clusters, 2D AoD, 2D AoA, initial phases of the four polarization combination state, amplitude, and XPR

²A cluster is defined as the path that can be resolved in the temporal domain. The number of rays in one path can be larger than the number of antenna elements in the array.

TABLE I
THE PARAMETERS IN THE DERIVATION AND THE CORRESPONDING DESCRIPTIONS

Notation	Description	Notation	Description
K	Number of total rays	L	Number of clusters
K_l	Ray number in cluster l	τ_l	Delay of cluster l
$\varphi_{r,lk}$	Azimuth AoA (AAoA) of the k_l th ray	$\varphi_{t,lk}$	Azimuth AoD (AAoD) of the k_l th ray
$\theta_{r,lk}$	Elevation AoA (EAoA) of the k_l th ray	$\theta_{t,lk}$	Elevation AoD (EAoD) of the k_l th ray
$\Theta_{t,lk}$	AoD angle pair of the k_l th ray	$\Theta_{r,lk}$	AoA angle pair of the k_l th ray
$\omega_{lk}^{hh}, \omega_{lk}^{hv}, \omega_{lk}^{vh}, \omega_{lk}^{vv}$	Initial phases of the k_l th ray	κ_{lk}	XPR of the k_l th ray
M_t	Transmitting NC-EMVA number	M_r	Receiving NC-EMVA number
\mathbf{g}_t	Gain vector of transmitting antenna array	\mathbf{g}_r	Gain vector of receiving antenna array
L_{seq}	Subsequence number	N_s	DFT point and subsequence length
N	Snapshot number	T	Symbol width

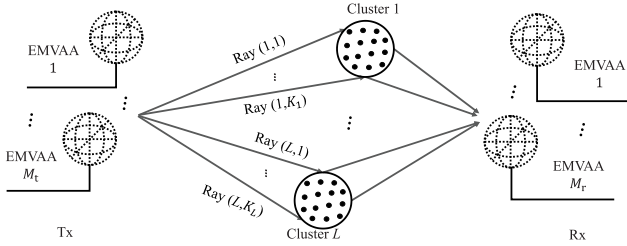


Fig. 1. Diagram of a CDL channel model.

of rays. These parameters are defined in this subsection. A total of K rays in L clusters are considered for the multipath environment, where $K = \sum_{l=1}^L K_l$, with K_l being the number of rays in the l th cluster. As shown in Fig. 1, the rays in the l th cluster arrive at the receiver with different AoDs and AoAs but approximately the same time delay τ_l . Denote the k th ray in the l th cluster as the k_l th ray. The azimuth AoA and AoD (AAoA and AAoD) of the k_l th ray are denoted by $\varphi_{r,lk}$ and $\varphi_{t,lk}$. The elevation AoA and AoD (EAoA and EAoD) of the k_l th ray are denoted by $\theta_{r,lk}$ and $\theta_{t,lk}$. The angle definition is given in Fig. 2 (b). Define $\Theta_{t,lk} \triangleq \{\varphi_{t,lk}, \theta_{t,lk}\}$ and $\Theta_{r,lk} \triangleq \{\varphi_{r,lk}, \theta_{r,lk}\}$. The direction cosine of AoD is denoted by

$$\mathbf{u}_{t,lk}(\Theta_{t,lk}) = [\sin\theta_{t,lk} \cos\varphi_{t,lk}, \sin\theta_{t,lk} \sin\varphi_{t,lk}, \cos\theta_{t,lk}]^T. \quad (1)$$

For the AoA, the direction cosine is $\mathbf{u}_{r,lk}(\Theta_{r,lk})$, which is obtained by substituting the subscript 't' in (1) with 'r'. The ray may change polarization status during propagation. Such a process is represented by

$$\mathbf{T}(\Xi_{lk}) = \begin{bmatrix} e^{j\omega_{lk}^{vv}} & \sqrt{\kappa_{lk}^{-1}} e^{j\omega_{lk}^{vh}} \\ \sqrt{\kappa_{lk}^{-1}} e^{j\omega_{lk}^{hv}} & e^{j\omega_{lk}^{hh}} \end{bmatrix} \quad (2)$$

where $\Xi_{lk} \triangleq \{\kappa_{lk}, \omega_{lk}^{hh}, \omega_{lk}^{hv}, \omega_{lk}^{vh}, \omega_{lk}^{vv}\}$ with $\{\omega_{lk}^{hh}, \omega_{lk}^{hv}, \omega_{lk}^{vh}, \omega_{lk}^{vv}\}$ being the different initial phases of the horizontal and vertical polarization combinations for the k_l th ray and κ_{lk} representing the XPR of the k_l th ray. The horizontal polarization is represented using \mathbf{h} , and \mathbf{v} for the vertical polarization. Note that XPR represents the power ratio of \mathbf{h} and \mathbf{v} polarization combinations for each ray due to scattering from the physical objects. As shown in Fig. 2(b),

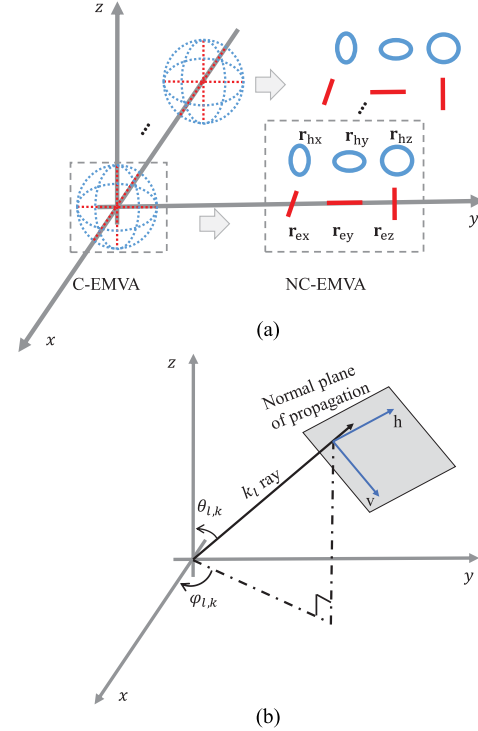


Fig. 2. EMVA configuration and angle definition. (a) Configuration of the C-EMVA and NC-EMVA; (b) Definition of the azimuth and elevation angles.

\mathbf{h} and \mathbf{v} are a set of orthogonal bases in the normal plane of the propagation direction [4].

B. Antenna Pattern and Array Configuration

In this work, a multipolarized MIMO system with M_t and M_r NC-EMVAs on the transmitting side and receiving side is considered. Fig. 2(a) shows the structure of the applied antenna arrays; the dashed lines depict the C-EMVA. The definitions of the azimuth and elevation angles are shown in Fig. 2(b). The coordinate of the m th C-EMVA can be denoted as $\mathbf{r}_m = [r_{m,x}, r_{m,y}, r_{m,z}]$. In addition, the reference coordinates of the six elements are given as \mathbf{r}_{ex} , \mathbf{r}_{ey} , \mathbf{r}_{ez} , \mathbf{r}_{hx} , \mathbf{r}_{hy} , and \mathbf{r}_{hz} for an NC-EMVA. In this study, the IES of the array can be larger than a half wavelength at the frequency of operation. Thus, the mutual coupling effect is effectively reduced, and the complicated array design is simplified.

In practical channel measurements, the gains of the transmit and receive antenna elements usually vary with the departure and incident angle. The antenna gains are taken into consideration in the received signal modeling progress to de-embed the influence of the antenna pattern. As shown in Fig. 2(a), the dipoles and loops are arranged in different directions for an NC-EMVA array (NC-EMVAA), so each element of an NC-EMVA has a unique antenna gain. Here, the gains of the transmitting NC-EMVA from Θ_t are denoted as $G_{t,ex}(\Theta_t)$, $G_{t,ey}(\Theta_t)$, $G_{t,ez}(\Theta_t)$, $G_{t,hx}(\Theta_t)$, $G_{t,hy}(\Theta_t)$ and $G_{t,hz}(\Theta_t)$. The gains vector of the transmitting antenna array for the k_l th ray is written as

$$\mathbf{g}_t(\Theta_{t,lk}) = [G_{t,ex}(\Theta_{t,lk}), G_{t,ey}(\Theta_{t,lk}), G_{t,ez}(\Theta_{t,lk}), G_{t,hx}(\Theta_{t,lk}), G_{t,hy}(\Theta_{t,lk}), G_{t,hz}(\Theta_{t,lk})]^T. \quad (3)$$

Similarly for the AoA, the gains are denoted by substituting the subscript 't' with 'r'. Let $\mathbf{a}_t(f, \Theta_{t,lk})$ be the $M_t \times 1$ space-frequency domain NC-EMVAA steering vector of the k_l th ray for the AoD. It can be expressed as

$$\mathbf{a}_t(f, \Theta_{t,lk}) = [e^{-j2\pi f \frac{r_{1,lt,k}}{c}}, \dots, e^{-j2\pi f \frac{r_{M_t,lt,k}}{c}}]^T \quad (4)$$

where c is the speed of light. For the AoA, it is denoted by $\mathbf{a}_r(f, \Theta_{r,lk})$.

Let $\mathbf{A}_{\text{pdt}}(f, \Theta_{t,lk})$ be the 6×2 SFP-domain steering matrix of the k_l th ray for an NC-EMVA in the transmitter. The 6 rows correspond to the 6 antenna elements of an NC-EMVA, and the 2 columns correspond to the polarization components along the v and h directions. It can be expressed as

$$\mathbf{A}_{\text{pdt}}(f, \Theta_{t,lk}) = \mathbf{D}_t(f, \Theta_{t,lk})\mathbf{\Omega}(\Theta_{t,lk}) \quad (5)$$

where $\mathbf{D}_t(f, \Theta_{t,lk})$ is the diagonal phase shift matrix of a NC-EMVA for the AoD, i.e.,

$$\mathbf{D}_t(f, \Theta_{t,lk}) = \text{diag}\{\mathbf{d}_{t,lk}(f, \Theta_{t,lk})\}. \quad (6)$$

The phase shift vector $\mathbf{d}_{t,lk}(f, \Theta_{t,lk})$ is denoted as (7), shown at the bottom of the page.

The space-polarization domain steering matrix for the C-EMVA is expressed as

$$\mathbf{\Omega}(\Theta_{t,lk}) = \begin{bmatrix} \cos \varphi_{t,lk} \cos \theta_{t,lk} & -\sin \varphi_{t,lk} & \\ \sin \varphi_{t,lk} \cos \theta_{t,lk} & \cos \varphi_{t,lk} & \\ -\sin \theta_{t,lk} & 0 & \\ -\sin \varphi_{t,lk} & -\cos \varphi_{t,lk} \cos \theta_{t,lk} & \\ \cos \varphi_{t,lk} & -\sin \varphi_{t,lk} \cos \theta_{t,lk} & \\ 0 & \sin \theta_{t,lk} & \end{bmatrix}. \quad (8)$$

For the AoA, the corresponding expressions are denoted by $\mathbf{A}_{\text{pdr}}(f, \Theta_{r,lk})$, $\mathbf{\Omega}(\Theta_{r,lk})$, $\mathbf{D}_r(f, \Theta_{r,lk})$ and $\mathbf{d}_{r,lk}(f, \Theta_{r,lk})$.

C. Transmit-Receive Signal Model

In this subsection, the transmit-receive signal model is analyzed. First, the transmitting sequence structure is designed.

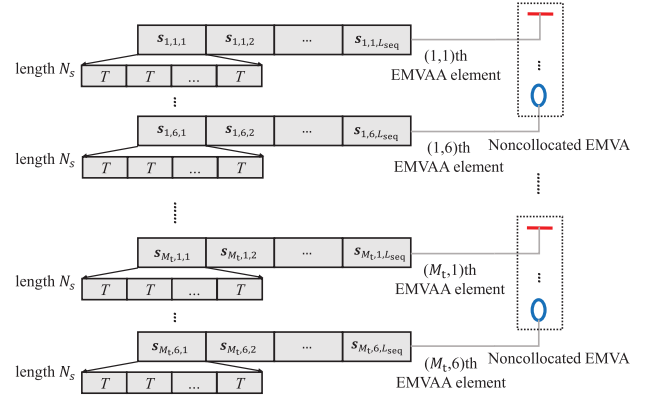


Fig. 3. Transmitting sequence structure of a snapshot.

Then, the receive signal model is given for the SFP-domain channel response derivation.

As shown in Fig. 3, there are $6M_t$ transmitting antenna elements respectively numbered (m_t, i) th antenna³, where $m_t = 1, \dots, M_t$ and $i = 1, \dots, 6$. The transmitting sequence of each antenna element is composed of L_{seq} subsequences. Note that $L_{\text{seq}} \geq 6M_t$. The length of each subsequence is N_s , which is also equal to the number of discrete Fourier transform (DFT) points. In practical implementations, the DFT uses fast Fourier transform (FFT). Then, the n_s th symbol of the l_{seq} th subsequence for (m_t, i) th transmitting antenna is denoted as $s_{m_t,i}[(l_{\text{seq}} - 1)N_s + n_s T]$ with $n_s = 1, \dots, N_s$ and $l_{\text{seq}} = 1, \dots, L_{\text{seq}}$, which is expressed as $s_{m_t,i,l_{\text{seq}}}(n_s T)$ with T being the symbol width for compact expression.

The transmitting sequences for all transmitting antennas in matrix form can be denoted as

$$\mathbf{S} = [\mathbf{S}_1, \mathbf{S}_2, \dots, \mathbf{S}_{L_{\text{seq}}}], \quad (9)$$

where \mathbf{S} is a $6M_t \times L_{\text{seq}}N_s$ matrix with $6M_t$ rows corresponding to the $6M_t$ transmitting antenna elements and $L_{\text{seq}}N_s$ columns corresponding to the L_{seq} subsequences with length N_s . The l_{seq} th subsequence for all transmitting antennas can be written as

$$\mathbf{S}_{l_{\text{seq}}} = [s_{l_{\text{seq}}1}, \dots, s_{l_{\text{seq}}N_s}] \quad (10)$$

where $s_{l_{\text{seq}}n_s}$ is the n_s th symbol of the l_{seq} th subsequence for all transmitting antennas, which is defined as

$$\mathbf{s}_{l_{\text{seq}}n_s} = [s_{1,1,l_{\text{seq}}}(n_s T), \dots, s_{M_t,6,l_{\text{seq}}}(n_s T)]^T. \quad (11)$$

After elaborating the transmitting sequence, the receive signal model is then described. Thus, the n_s sample of the l_{seq} th subsequence in the n th snapshot of the received signal can be denoted by (12), where \mathbf{z}_n is the complex white Gaussian noise of the n th snapshot and $\alpha_{n,lk}$ represents the amplitude of the k_l th ray in the n th snapshot. The channel is considered as time-varying for different snapshots. The received signal is obtained by summarizing the signal carried by all rays.

³The (m_t, i) th antenna is defined as the i th element of the m_t th NC-EMVA.

$$\mathbf{d}_{t,lk}(f, \Theta_{t,lk}) = [e^{-j2\pi f \frac{r_{\text{ex}} \mathbf{u}_{t,lk}}{c}}, e^{-j2\pi f \frac{r_{\text{ey}} \mathbf{u}_{t,lk}}{c}}, e^{-j2\pi f \frac{r_{\text{ez}} \mathbf{u}_{t,lk}}{c}}, e^{-j2\pi f \frac{r_{\text{hx}} \mathbf{u}_{t,lk}}{c}}, e^{-j2\pi f \frac{r_{\text{hy}} \mathbf{u}_{t,lk}}{c}}, e^{-j2\pi f \frac{r_{\text{hz}} \mathbf{u}_{t,lk}}{c}}]^T. \quad (7)$$

The remaining variables used in (12) and their corresponding descriptions can be found in Table I.

$$\begin{aligned}
& \mathbf{y}_{n n_s l_{\text{seq}}} (f, \Theta_r, \Theta_t, \Xi) \\
&= \sum_{l=1}^L \sum_{k=1}^{K_l} \alpha_{n, lk} \mathbf{a}_r (f, \Theta_r, lk) \\
& \quad \otimes [\mathbf{g}_r^T (\Theta_r, lk) \oplus \mathbf{A}_{\text{pdr}}^T (f, \Theta_r, lk)]^T \mathbf{T} (\Xi_{lk}) \mathbf{a}_t^T (f, \Theta_t, lk) \\
& \quad \otimes [\mathbf{g}_t^T (\Theta_t, lk) \oplus \mathbf{A}_{\text{pdt}}^T (f, \Theta_t, lk)] \mathbf{s}_{l_{\text{seq}} n_s} (n_s T - \tau_l) + \mathbf{z}_n
\end{aligned} \quad (12)$$

D. Channel Response in the SFP Domain

In this subsection, the channel response in the SFP domain is derived via the received signal. Let $\mathbf{Y}_{n l_{\text{seq}}}$ be the received signal of the l_{seq} th transmitting signal in the n th snapshot, i.e.,

$$\mathbf{Y}_{n l_{\text{seq}}} = [\mathbf{y}_{n 1 l_{\text{seq}}}, \mathbf{y}_{n 2 l_{\text{seq}}}, \dots, \mathbf{y}_{n N_s l_{\text{seq}}}] \quad (13)$$

where $\mathbf{Y}_{n l_{\text{seq}}} (f, \Theta_t, \Theta_r, \Xi)$ and $\mathbf{y}_{n n_s l_{\text{seq}}} (f, \Theta_t, \Theta_r, \Xi)$ are replaced by $\mathbf{Y}_{n l_{\text{seq}}}$ and $\mathbf{y}_{n n_s l_{\text{seq}}}$ for simplicity, respectively. Performing the DFT on each row of $\mathbf{Y}_{n l_{\text{seq}}} \in \mathbb{C}^{6M_r \times N_s}$ yields

$$\mathbf{Y}_{n l_{\text{seq}} f} = [\mathbf{y}_{n l_{\text{seq}} f_1}, \mathbf{y}_{n l_{\text{seq}} f_2}, \dots, \mathbf{y}_{n l_{\text{seq}} f_{N_s}}], \quad (14)$$

where $\mathbf{Y}_{n l_{\text{seq}} f} \in \mathbb{C}^{6M_r \times N_s}$ is the SFP-domain received signal of the l_{seq} th subsequence in snapshot n . There are L_{seq} subsequences in total. DFT is performed on each subsequence, and the SFP-domain received signal in frequency bin f_i is selected. Then, the received signal of the n th snapshot in frequency bin f_i $\mathbf{Y}_{n f_i} \in \mathbb{C}^{6M_r \times L_{\text{seq}}}$ can be obtained as

$$\mathbf{Y}_{n f_i} = [\mathbf{y}_{n 1 f_i}, \mathbf{y}_{n 2 f_i}, \dots, \mathbf{y}_{n L_{\text{seq}} f_i}] = \mathbf{H}_{n f_i} \tilde{\mathbf{S}}_{f_i} + \mathbf{Z}_{n f_i}, \quad (15)$$

where $\mathbf{H}_{n f_i} \in \mathbb{C}^{6M_r \times 6M_t}$ and $\mathbf{Z}_{n f_i}$ respectively represent the channel response matrix and additive white Gaussian noise (AWGN) matrix in the n th snapshot in frequency bin f_i . The standard deviation of the noise is σ_n with mean zero. $\tilde{\mathbf{S}}_{f_i} \in \mathbb{C}^{6M_t \times L_{\text{seq}}}$ is the frequency domain transmitting signal in frequency bin f_i for all subsequences, which can be expressed as

$$\tilde{\mathbf{S}}_{f_i} = [\mathbf{S}_1 \mathcal{F}, \mathbf{S}_2 \mathcal{F}, \dots, \mathbf{S}_{L_{\text{seq}}} \mathcal{F}] \mathbf{J}_{f_i} \quad (16)$$

where \mathcal{F} stands for the DFT matrix and \mathbf{J}_{f_i} is the selection matrix that selects the signal of the frequency bin f_i , which is defined as $\mathbf{J}_{f_i} = \mathbf{I}_{L_{\text{seq}}} \otimes \mathbf{e}_i$. It is easy to design a signal matrix $\tilde{\mathbf{S}}_{f_i}$ with full row rank. $\mathbf{H}_{n f_i}$ is the basic component of the SFP channel response in frequency bin f_i and snapshot n . Therefore, it is vital to analyze the derivation of $\mathbf{H}_{n f_i}$. According to (12) and (15), $\mathbf{H}_{n f_i}$ is expressed as

$$\begin{aligned}
\mathbf{H}_{n f_i} &= \sum_{l=1}^L \sum_{k=1}^{K_l} e^{-j2\pi f_i \tau_l} \alpha_{n, lk} \mathbf{a}_r (f_i, \Theta_r, lk) \\
& \quad \otimes [\mathbf{g}_r^T (\Theta_r, lk) \oplus \mathbf{A}_{\text{pdr}}^T (f_i, \Theta_r, lk)]^T \mathbf{T} (\Xi_{lk}) \\
& \quad \otimes \mathbf{a}_t^T (f_i, \Theta_t, lk) [\mathbf{g}_t^T (\Theta_t, lk) \oplus \mathbf{A}_{\text{pdt}}^T (f_i, \Theta_t, lk)] \quad (17)
\end{aligned}$$

For simplicity of expression, $\mathbf{a}_r (f_i, \Theta_r, lk)$, $\mathbf{g}_r (\Theta_r, lk)$ and $\mathbf{A}_{\text{pdr}} (f_i, \Theta_r, lk)$ will be denoted by $\mathbf{a}_{r f_i, lk}$, $\mathbf{g}_{r, lk}$ and $\mathbf{A}_{\text{pdr} f_i, lk}$ in the following derivations. Similar simplified expressions

are also applied in $\mathbf{a}_{t f_i, lk}$, $\mathbf{g}_{t, lk}$ and $\mathbf{A}_{\text{pdt} f_i, lk}$. Define $\mathbf{A}_{t f_i, lk} \in \mathbb{C}^{6M_t \times 2}$ as the transmitting array steering matrix of the k_l th ray in frequency bin f_i , which is denoted as

$$\mathbf{A}_{t f_i, lk} = \mathbf{a}_{t f_i, lk} \otimes [\mathbf{g}_{t, lk}^T \oplus \mathbf{A}_{\text{pdt} f_i, lk}^T]^T. \quad (18)$$

The corresponding receiving array steering matrix is denoted by substituting the subscript 't' in (18) with 'r'. Let $\mathbf{h}_{n f_i} = \text{vec}\{\mathbf{H}_{n f_i}\}$. After vectorization, $\mathbf{h}_{n f_i} \in \mathbb{C}^{36M_t M_r \times 1}$ can be expressed as

$$\mathbf{h}_{n f_i} = \sum_{l=1}^L \sum_{k=1}^{K_l} \alpha_{n, lk} e^{-j2\pi f_i \tau_l} \mathbf{b}_{t r f_i, lk} \quad (19)$$

where $\mathbf{b}_{t r f_i, lk} \in \mathbb{C}^{36M_t M_r \times 1}$ is the steering vector of the k_l th ray in frequency bin f_i given as

$$\mathbf{b}_{t r f_i, lk} = \mathbf{A}_{t r f_i, lk} \beta_{lk}. \quad (20)$$

Here, $\mathbf{A}_{t r f_i, lk} \in \mathbb{C}^{36M_t M_r \times 4}$ is the steering matrix of the k_l th ray in frequency bin f_i , which is defined as

$$\mathbf{A}_{t r f_i, lk} = \mathbf{A}_{t f_i, lk} \otimes \mathbf{A}_{r f_i, lk} \quad (21)$$

In (20), $\beta_{lk} = \text{vec}\{\mathbf{T}_{lk}\}$ is a column vector. For compact expression, let us rewrite (19) as

$$\mathbf{h}_{n f_i} = \mathbf{B}_{t r f_i} \mathbf{F}_{f_i} \alpha_n = \mathbf{B}_{f_i} \alpha_n \quad (22)$$

where

$$\mathbf{B}_{t r f_i} = [\mathbf{b}_{t r f_i, 11}, \dots, \mathbf{b}_{t r f_i, 1K_1}, \dots, \mathbf{b}_{t r f_i, L1}, \dots, \mathbf{b}_{t r f_i, LK_L}] \quad (23)$$

and α_n is the amplitude vector for all rays in snapshot n denoted as

$$\alpha_n = [\alpha_{n, 11}, \dots, \alpha_{n, 1K_1}, \dots, \alpha_{n, LK_L}, \dots, \alpha_{n, LK_L}]^T. \quad (24)$$

In (22), $\mathbf{F}_{f_i} \in \mathbb{C}^{K \times K}$ is the phase shifting diagonal matrix of frequency bin f_i caused by the delay written as

$$\mathbf{F}_{f_i} = \text{diag}\{[e^{-j2\pi f_i \tau_1} \otimes \mathbf{1}_{1 \times K_1}, \dots, e^{-j2\pi f_i \tau_L} \otimes \mathbf{1}_{1 \times K_L}]\}. \quad (25)$$

Then, \mathbf{h}_{n, f_i} can be estimated as

$$\hat{\mathbf{h}}_{n f_i} = \text{vec}\{\mathbf{Y}_{n f_i} \tilde{\mathbf{S}}_{f_i}^\dagger\}. \quad (26)$$

Thus, the estimated channel response in the SFP domain for all frequency bins and snapshots $\hat{\mathbf{H}} \in \mathbb{C}^{36M_t M_r N_s \times N}$ can be obtained as

$$\hat{\mathbf{H}} = \begin{bmatrix} \hat{\mathbf{h}}_{1 f_1} & \hat{\mathbf{h}}_{2 f_1} & \cdots & \hat{\mathbf{h}}_{N f_1} \\ \hat{\mathbf{h}}_{1 f_2} & \hat{\mathbf{h}}_{2 f_2} & \cdots & \hat{\mathbf{h}}_{N f_2} \\ \vdots & \vdots & \ddots & \vdots \\ \hat{\mathbf{h}}_{1 f_{N_s}} & \hat{\mathbf{h}}_{2 f_{N_s}} & \cdots & \hat{\mathbf{h}}_{N f_{N_s}} \end{bmatrix} \quad (27)$$

which can be further expressed as

$$\hat{\mathbf{H}} = \mathbf{B} \mathbf{\Gamma} + \hat{\mathbf{Z}} \quad (28)$$

where $\mathbf{B} \in \mathbb{C}^{36M_t M_r N_s \times K}$, $\mathbf{\Gamma}$ and $\hat{\mathbf{Z}}$ respectively represent the steering matrix of the array, the amplitude of rays for N snapshots and the noise matrix, which are given as

$$\mathbf{B} = [\mathbf{B}_{f_1}^T, \mathbf{B}_{f_2}^T, \dots, \mathbf{B}_{f_{N_s}}^T]^T, \quad (29)$$

$$\mathbf{\Gamma} = [\alpha_1, \dots, \alpha_N], \quad (30)$$

and

$$\hat{\mathbf{Z}} = \begin{bmatrix} \text{vec}(\mathbf{Z}_{1f_1} \mathbf{S}_{f_1}^\dagger) & \cdots & \text{vec}(\mathbf{Z}_{Nf_1} \mathbf{S}_{f_1}^\dagger) \\ \vdots & \ddots & \vdots \\ \text{vec}(\mathbf{Z}_{1f_{N_s}} \mathbf{S}_{f_{N_s}}^\dagger) & \cdots & \text{vec}(\mathbf{Z}_{Nf_{N_s}} \mathbf{S}_{f_{N_s}}^\dagger) \end{bmatrix}. \quad (31)$$

III. MULTIPARAMETER ESTIMATION

A. Maximum Likelihood Estimator

The maximum likelihood estimator is considered an accurate estimator. The likelihood function can be written compactly as

$$L(\boldsymbol{\tau}, \boldsymbol{\Theta}_t, \boldsymbol{\Theta}_r, \boldsymbol{\Xi}) = \arg \max_{\boldsymbol{\tau}, \boldsymbol{\Theta}_t, \boldsymbol{\Theta}_r, \boldsymbol{\Xi}} \{M_t M_r N_s \ln F(\boldsymbol{\tau}, \boldsymbol{\Theta}_t, \boldsymbol{\Theta}_r, \boldsymbol{\Xi})\} \quad (32)$$

where

$$F(\boldsymbol{\tau}, \boldsymbol{\Theta}_t, \boldsymbol{\Theta}_r, \boldsymbol{\Xi}) = \text{tr} \left\{ \hat{\mathbf{H}} \hat{\mathbf{H}}^H - \mathbf{B}(\boldsymbol{\tau}, \boldsymbol{\Theta}_t, \boldsymbol{\Theta}_r, \boldsymbol{\Xi}) \mathbf{B}^\dagger(\boldsymbol{\tau}, \boldsymbol{\Theta}_t, \boldsymbol{\Theta}_r, \boldsymbol{\Xi}) \hat{\mathbf{H}} \hat{\mathbf{H}}^H \right\}. \quad (33)$$

Thus, the ML estimate of $\boldsymbol{\tau}$, $\boldsymbol{\Theta}_t$, $\boldsymbol{\Theta}_r$ and $\boldsymbol{\Xi}$ is obtained by maximizing $F(\boldsymbol{\tau}, \boldsymbol{\Theta}_t, \boldsymbol{\Theta}_r, \boldsymbol{\Xi})$. Due to the large number of impinging rays and multiple parameters, the ML estimator consumes substantial computational resources. Therefore, it is proposed that these multiple parameters are estimated one after the other to reduce computational complexity.

B. Delay and Angle Estimation

In this subsection, the delay and angle estimation method is derived. The propagation delay of a ray is estimated from the frequency domain channel response of the reference antenna element. In this work, the first antenna element of the first NC-EMVA is selected as the reference antenna element of the transmitting and receiving antenna array. Define a selection matrix $\mathbf{J}_\tau = \mathbf{I}_{N_s} \otimes \mathbf{e}_1^T$, where \mathbf{e}_1 is the first column of $\mathbf{I}_{36M_r M_t}$. The role of the selection matrix \mathbf{J}_τ is to select the channel response of the reference antenna element from the SFP-domain channel response. Then, the selection progress is expressed as

$$\hat{\mathbf{H}}_\tau = \mathbf{J}_\tau \hat{\mathbf{H}}. \quad (34)$$

Let $\hat{\mathbf{R}}_\tau = \frac{1}{N} \hat{\mathbf{H}}_\tau \hat{\mathbf{H}}_\tau^H$ be the covariance matrix of $\hat{\mathbf{H}}_\tau$. The rank of $\hat{\mathbf{R}}_\tau$ is the number of clusters without considering the noise. The eigenvalue decomposition (EVD) of $\hat{\mathbf{R}}_\tau$ leads to the $N_s \times (N_s - L)$ noise subspace $\mathbf{U}_{n,\tau}$. The delay MUSIC estimation can be expressed as

$$P_\tau(\tau) = \arg \min_{\tau} |\mathbf{a}_\tau^H(\tau) \mathbf{U}_{n,\tau} \mathbf{U}_{n,\tau}^H \mathbf{a}_\tau(\tau)| \quad (35)$$

where \mathbf{a}_τ is the steering vector in the frequency domain of the reference antenna element, which can be expressed as

$$\mathbf{a}_\tau(\tau) = [e^{-j2\pi f_1 \tau}, e^{-j2\pi f_2 \tau}, \dots, e^{-j2\pi f_{N_s} \tau}]^T. \quad (36)$$

With the delay estimated by the above MUSIC technique, the angle estimation is then processed. The AoD can be estimated with the channel response related to the transmitting

antenna elements and the reference receiving antenna element. Define a selection matrix $\mathbf{J}_t = \mathbf{I}_{6N_s M_t} \otimes \mathbf{e}_1^T$, where \mathbf{e}_1 is the first column of \mathbf{I}_{6M_r} . The role of the selection matrix \mathbf{J}_t is to select the channel response of the transmitting antennas and the reference receiving antenna element from the SFP-domain channel response. Then, the selected channel response is given as

$$\hat{\mathbf{H}}_t = \mathbf{J}_t \hat{\mathbf{H}} = \tilde{\mathbf{B}}_t \boldsymbol{\Gamma} + \mathbf{J}_t \hat{\mathbf{Z}} \quad (37)$$

where $\tilde{\mathbf{B}}_t$ is the steering matrix of the transmitting array channel response, i.e.,

$$\tilde{\mathbf{B}}_t = [(\tilde{\mathbf{B}}_{f_1} \mathbf{F}_{f_1})^T, \dots, (\tilde{\mathbf{B}}_{f_{N_s}} \mathbf{F}_{f_{N_s}})^T]^T. \quad (38)$$

Here, $\tilde{\mathbf{B}}_{f_i}$ is obtained as

$$\tilde{\mathbf{B}}_{f_i} = \mathbf{J}_{t,\text{ref}} \mathbf{B}_{f_i} \quad (39)$$

where $\mathbf{J}_{t,\text{ref}} = \mathbf{I}_{6M_t} \otimes \mathbf{e}_1^T$ with the length of \mathbf{e}_1 being $6M_r$. The role of the selection matrix $\mathbf{J}_{t,\text{ref}}$ is to select the channel response of the transmitting antennas from the SFP-domain channel response in any frequency bin. Let $\hat{\mathbf{R}}_t = \frac{1}{N} \hat{\mathbf{H}}_t \hat{\mathbf{H}}_t^H$ be the covariance matrix of $\hat{\mathbf{H}}_t$. The rank of $\hat{\mathbf{R}}_t$ is equal to the number of rays without considering the noise. The EVD of $\hat{\mathbf{R}}_t$ leads to the $6M_t N_s \times (6M_t N_s - K)$ noise subspace \mathbf{U}_{tn} . The estimated AoD can be obtained by

$$\hat{\Theta}_{t,lk} = \arg \min_{\Theta_{t,lk}} \{P_t(\Theta_{t,lk})\}, \quad (40)$$

where $P_t(\Theta_{t,lk})$ is the AoD MUSIC spectrum,

$$P_t(\Theta_{t,lk}) = \det \{ |\mathbf{A}_{t,lk}^H(\Theta_{t,lk}) \mathbf{U}_{tn} \mathbf{U}_{tn}^H \mathbf{A}_{t,lk}(\Theta_{t,lk})| \}. \quad (41)$$

The expression of $\mathbf{A}_{t,lk}$ and the corresponding derivation process are shown in Appendix A.

Similarly, the AoA is estimated with the channel response related to the receiving antenna elements and the reference transmitting antenna element. Define a selection matrix $\mathbf{J}_r = \mathbf{I}_{N_s} \otimes \mathbf{e}_1^T \otimes \mathbf{I}_{6M_r}$, where \mathbf{e}_1 is the first column of \mathbf{I}_{6M_t} . Then, the receiving array channel response is

$$\hat{\mathbf{H}}_r = \mathbf{J}_r \hat{\mathbf{H}} = \tilde{\mathbf{B}}_r \boldsymbol{\Gamma} + \mathbf{J}_r \hat{\mathbf{Z}} \quad (42)$$

where $\tilde{\mathbf{B}}_r$ is the steering matrix of the receiving array channel response, i.e.,

$$\tilde{\mathbf{B}}_r = [(\tilde{\mathbf{B}}_{f_1} \mathbf{F}_{f_1})^T, \dots, (\tilde{\mathbf{B}}_{f_{N_s}} \mathbf{F}_{f_{N_s}})^T]^T. \quad (43)$$

Here, $\tilde{\mathbf{B}}_{f_i}$ is obtained as

$$\tilde{\mathbf{B}}_{f_i} = \mathbf{J}_{r,\text{ref}} \mathbf{B}_{f_i} \quad (44)$$

where $\mathbf{J}_{r,\text{ref}} = \mathbf{e}_1^T \otimes \mathbf{I}_{6M_r}$ with the length of \mathbf{e}_1 being $6M_t$. Note that $\tilde{\mathbf{B}}_{f_i}$ in AoA estimation is different from that in AoD estimation, which is caused by the different selection matrices $\mathbf{J}_{t,\text{ref}}$ and $\mathbf{J}_{r,\text{ref}}$. Let $\hat{\mathbf{R}}_r = \frac{1}{N} \hat{\mathbf{H}}_r \hat{\mathbf{H}}_r^H$ be the covariance matrix of $\hat{\mathbf{H}}_r$. The rank of $\hat{\mathbf{R}}_r$ is equal to the number of rays without considering the noise. The EVD of $\hat{\mathbf{R}}_r$ leads to the $6M_r N_s \times (6M_r N_s - K)$ noise subspace \mathbf{U}_{rn} . The estimated AoA can be obtained by

$$\hat{\Theta}_{r,lk} = \arg \min_{\Theta_{r,lk}} \{P_r(\Theta_{r,lk})\}, \quad (45)$$

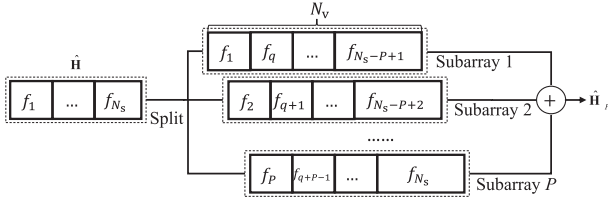


Fig. 4. Diagram of the subarray division method.

where $P_r(\Theta_{r,lk})$ is the AoA MUSIC spectrum,

$$P_r(\Theta_{r,lk}) = \det \{ |\mathbf{A}_r^H(\Theta_{r,lk}) \mathbf{U}_{rn} \mathbf{U}_{rn}^H \mathbf{A}_r(\Theta_{r,lk})| \}. \quad (46)$$

C. Frequency Domain Smoothing Technique

In the application of the BEAR-based method, the FFT points are usually too large to perform EVD on the covariance matrix of the channel response. To reduce the effect of the AWGN and the computational complexity, a frequency domain smoothing preprocessing technique is proposed. The whole frequency band is divided into P subfrequency bands, and each subfrequency band corresponds to a virtual subarray. The number of frequency bins in each subfrequency band is N_v . And N_v should meet the condition $\min\{6M_t N_v, 6M_r N_v\} > K$. The difference in frequency bins in the adjacent subarray is the DFT frequency interval. Then, the channel impulse responses of all the virtual subarrays are summarized. Fig. 4 shows a diagram of the virtual subarray division. The closed-form MUSIC spectra of the AoD and AoA can be derived by means of this technique. See Appendix B for details of the derivation process.

D. Pair Matching of AoD and AoA

The estimated AoD and AoA must be paired. The channel response in any frequency bin, for example, the top $36M_r M_t$ rows of \mathbf{H} , can be used to perform pair matching. Let $\mathbf{H}_{\text{pair}} = \mathbf{J}_{\text{pair}} \mathbf{H}$, where $\mathbf{J}_{\text{pair}} = \mathbf{e}_1^T \otimes \mathbf{I}_{N_s}$ with the length of \mathbf{e}_1 being $36M_r M_t$. EVD of \mathbf{H}_{pair} yields the noise subspace $\mathbf{U}_{\text{pair},n}$.

The steering matrix for the channel response of the selected frequency bin is constructed as

$$\mathbf{A}_{\text{pair}}(\hat{\Theta}_{r,lk}, \hat{\Theta}_{t,lk}) = \mathbf{A}_{t,f_1,lk}(\hat{\Theta}_{t,lk}) \otimes \mathbf{A}_{r,f_1,lk}(\hat{\Theta}_{r,lk}). \quad (47)$$

The aim of the pair matching of AoD and AoA is to find the AoD-AoA pair such that

$$P_{\text{pair}} = \arg \min_{\hat{\Theta}_{r,lk}, \hat{\Theta}_{t,lk}} \det \{ |\mathbf{A}_{\text{pair}}^H \mathbf{U}_{\text{pair},n} \mathbf{U}_{\text{pair},n}^H \mathbf{A}_{\text{pair}}| \}. \quad (48)$$

E. Estimation of Initial Phases, XPR and Amplitude

With the estimated delay and paired angles of the rays, the remaining parameters, XPR, amplitude and initial phases can be estimated. Let

$$\mathbf{A} = \begin{bmatrix} e^{-j2\pi f_1 \tau_1} \mathbf{A}_{t,f_1,11} & \cdots & e^{-j2\pi f_1 \tau_L} \mathbf{A}_{t,f_1,LK_L} \\ \vdots & \ddots & \vdots \\ e^{-j2\pi f_N \tau_L} \mathbf{A}_{t,f_N,11} & \cdots & e^{-j2\pi f_N \tau_L} \mathbf{A}_{t,f_N,LK_L} \end{bmatrix}. \quad (49)$$

TABLE II
STEPS OF THE BEAR-BASED SUBSPACE ESTIMATOR

Steps of delay, AoD, AoA, initial phases, XPR and amplitude estimation
1: for $n = 1$ to N do
2: Perform FFT on the received signals of the n th snapshot.
3: Calculate the channel response of each frequency bin as (26).
4: Vectorize the channel response matrix as the n th column of (27).
5: end for
6: Calculate $\hat{\mathbf{H}}_r$ as (34), then estimate the delay using (35).
7: for $l = 1$ to L do
8: Calculate $\hat{\mathbf{H}}_t$ and $\hat{\mathbf{H}}_r$, then perform frequency smoothing to obtain $\mathbf{H}_{t,P}$ and $\mathbf{H}_{r,P}$, estimate AoD using (66).
9: end for
10: Perform pair matching between AoD and AoA.
11: Estimate initial phases, XPR and amplitude with (52), (53) and (54).

The steering matrix of the array \mathbf{B} can be rewritten as $\mathbf{B} = \mathbf{A}\Psi$, where Ψ is the block diagonal matrix, and can be expressed as

$$\Psi = \mathbf{I}_K \oplus [\beta_{11}, \dots, \beta_{1K_1}, \dots, \beta_{L1}, \dots, \beta_{LK_L}]. \quad (50)$$

Then, $\mathbf{\Pi} = \Psi\mathbf{\Gamma}$ can be obtained with the estimated delay and angle as $\hat{\mathbf{\Pi}} = \hat{\mathbf{A}}^\dagger \hat{\mathbf{H}}$. To reduce the effect of the noise, sum $\hat{\mathbf{\Pi}}$ by column to obtain a column vector denoted by \mathbf{v} , which can be written as

$$\begin{aligned} \mathbf{v} &= [\mathbf{v}_{11}^T, \dots, \mathbf{v}_{LK_L}^T]^T \\ &= \left[\sum_{n=1}^N \alpha_{n,11} \beta_{11}^T, \dots, \sum_{n=1}^N \alpha_{n,LK_L} \beta_{LK_L}^T \right]^T. \end{aligned} \quad (51)$$

Let ω be the initial phase vector of all rays $\omega = [\omega_{11}^{vv}, \omega_{11}^{hv}, \omega_{11}^{vh}, \omega_{11}^{hh}, \dots, \omega_{LK_L}^{vv}, \omega_{LK_L}^{hv}, \omega_{LK_L}^{vh}, \omega_{LK_L}^{hh}]^T$. Then, the estimate of ω can be written as

$$\hat{\omega} = \arg\{\mathbf{v}\}. \quad (52)$$

For the k_l th ray, the XPR can be estimated as

$$\hat{\kappa}_{lk} = \left(\frac{|\mathbf{v}_{lk}(1)| + |\mathbf{v}_{lk}(4)|}{|\mathbf{v}_{lk}(2)| + |\mathbf{v}_{lk}(3)|} \right)^2. \quad (53)$$

With the estimated initial phase and XPR, Ψ can be reconstructed as $\hat{\Psi}$; then the amplitude of the rays for all N snapshots is estimated as

$$\hat{\mathbf{\Gamma}} = \hat{\Psi}^\dagger \hat{\mathbf{\Pi}}. \quad (54)$$

F. Derivation of the Cramer-Rao Lower Bound (CRLB)

The method of CRLB derivation in [30] is used in this work. The parameters that must be estimated are $(\varphi_{t,lk}, \theta_{t,lk}, \varphi_{r,lk}, \theta_{r,lk}, \tau_l)$, with $l = 1, \dots, L$ and $k = 1, \dots, K_L$. The CRLB is given as

$$\text{CRLB}(\vartheta) = \frac{\sigma_n}{2} \left(\sum_{n=1}^N \text{Re} \{ \mathbf{\Lambda}_n^H \mathbf{\Upsilon}^H (\mathbf{I} - \mathbf{B}\mathbf{B}^\dagger) \mathbf{\Upsilon} \mathbf{\Lambda}_n \} \right)^{-1} \quad (55)$$

where ϑ represents one of the parameters to be estimated, $\mathbf{\Lambda}_n = \text{diag}\{\alpha_{n,lk}\}$, and $\mathbf{\Upsilon}$ is given in Appendix C.

TABLE III
COMPARISONS OF THE PROPOSED BEAR-BASED SUBSPACE ESTIMATION METHOD WITH THOSE IN THE REFERENCES

Method	Estimated parameters	Number of resolvable rays in one cluster
JSTPE [24]	Delay, AAoA	$6M_r - 1$
SAGE [22]	Delay, AAoA, Amplitude	-
MAPS [23]	Delay, 2D AoA	$6M_r - 1$
Proposed Method	Delay, 2D AoA, 2D AoD, XPR Amplitude, Initial Phases	$6M_r N_s / P - 1$

TABLE IV
COMPLEXITY ANALYSIS OF THE PROPOSED METHOD

Operation	Computational complexity
FFT for the received signals	$O(3N L_{\text{seq}} N_s M_r \log_2 N_s)$
EVD of \mathbf{H}_τ	$O(N_s^3)$
MUSIC delay search	$O(LW_\tau N_s^2)$
EVD of \mathbf{H}_r	$O(216M_r^3 N_v^3)$
EVD of \mathbf{H}_t	$O(216M_t^3 N_v^3)$
MUSIC AoA search	$O(48LW_{\text{AoA}} M_r N_v (3M_r N_v + 2))$
MUSIC AoD search	$O(48LW_{\text{AoD}} M_t N_v (3M_t N_v + 2))$

G. Implementation of the Bear-Based Subspace Method and Comparisons With Existing Methods

The multiparameter estimation procedure using the BEAR-based subspace method is summarized in Table II. Comparisons with existing methods are presented in Table III. The existing methods cannot resolve rays in the same cluster when the number of rays is greater than the number of antenna elements. For the genuine SAGE algorithm, the resolvable rays are not given clearly, but the low robustness caused by overlapping signals in the temporal domain and algorithm complexity limit its practical implementation. Even so, the SAGE algorithm in [22] is still a widely used algorithm for channel parameter estimation. It is suitable for time invariant channel environments and specular rays extraction. For researchers are interested in the AoA and delay, the SAGE algorithm is a nice candidate approach. However, when researchers are interested in not only the delay and AoA parameters but also the other parameters in 3GPP, BEAR is a potential candidate parameter estimation approach.

H. Complexity Analysis

The computational complexity of the proposed method is calculated in terms of complex multiplications. To reduce the computational burden, the N -point DFT uses the FFT algorithm with computational complexity of $\frac{N}{2} \log_2 N$. The computational complexity for an EVD of an $M \times M$ matrix is $O(M^3)$. In Table IV, the complexity of estimating the parameters for all K rays is shown in detail where W_τ , W_{AoD} and W_{AoA} represent the number of rank-deficient MUSIC search times, W_τ is the one-dimensional search times, which is inversely proportional to the search step, and W_{AoD} and W_{AoA} are 2D search times, which are inversely proportional to the square of the search step. The AoD and AoA estimation is based on the delay of clusters. Thus, the search process needs to be performed L times.

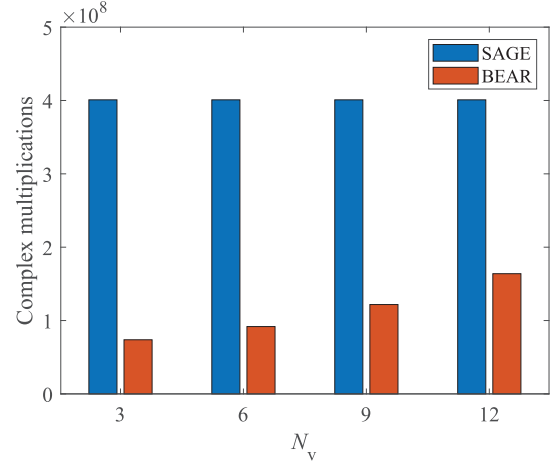


Fig. 5. Complexity comparisons of the proposed BEAR with the SAGE algorithm.

To give a more intuitive complexity analysis, the computational complexity of the proposed algorithm is compared with the one of the SAGE algorithm in Fig. 5. The complexity of the SAGE algorithm relies on the number of iteration cycles which is assumed to be 2 here. In actual applications, the number of iteration cycles is affected by the initial values and the convergence speed, which is usually larger than 2. It is easy to find that the complexity of the BEAR is directly related to the virtual subarray size N_v .

I. Notifications in BEAR Application

In the above subsections, the BEAR-based subspace multiparameter estimation method is analyzed. Two points warrant further discussion.

The first is the selection of the frequency bins in virtual subarray 1. To avoid correlations between the steering vectors of the rays in different clusters, the minimum frequency bins interval $\Delta \tilde{f}$ in virtual subarray 1 needs to meet the following conditions:

$$\Delta \tilde{f} \tau_{\max} < 1 \quad (56)$$

where τ_{\max} is the maximum delay of all clusters.

The second is the selection of virtual subarray numbers P . The frequency domain smoothing procedure is not an in-phase summation progress in (62) and (63). By smoothing the receiving signals, the SNR gain is expressed by [31]

$$\text{SNR}_{\text{sm}}(P) = \frac{1}{P} \left| \frac{1 - e^{-j2\pi P \Delta f \tau_l}}{1 - e^{-j2\pi \Delta f \tau_l}} \right|^2 \quad (57)$$

Then, the optimal P is obtained by maximizing (57).

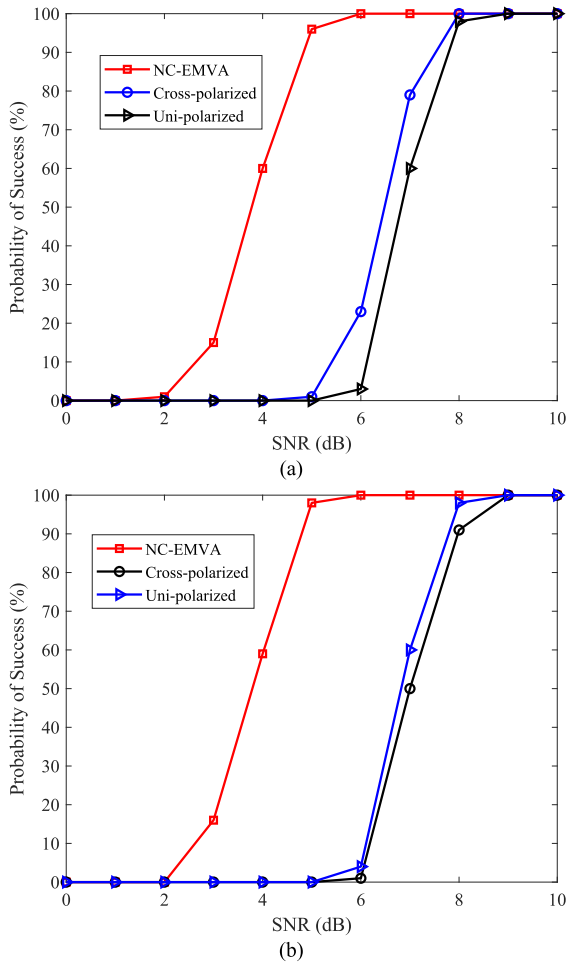


Fig. 6. The probability of success for AoD and AoA using different polarized antenna arrays. (a) AoD; (b) AoA.

IV. NUMERICAL SIMULATIONS AND ANALYSIS

In this section, simulations are performed to show the performance of the proposed BEAR-based subspace estimation method. Multipath propagation channels with additive white Gaussian noises are used. First, the performance of different polarized arrays in the 6×6 MIMO system is given to demonstrate the advantages of the NC-EMVAA. Next, the detailed simulation setup for the comprehensive simulations is given. Then, the comprehensive simulation results of the proposed algorithm are shown. Furthermore, The probability of success and the RMSE of angle estimation are investigated in detail. The XPR, initial phases, and amplitude estimation results are finally given.

In the simulation, high performance of the proposed BEAR-based method is achieved under different SNRs and array sizes. To evaluate the estimation accuracy, the root mean square error (RMSE) of the angle estimation is given as

$$\text{RMSE} = \sqrt{\frac{1}{KQ} \sum_{q=1}^Q \sum_{l=1}^L \sum_{k=1}^{K_l} (\hat{\xi}_{lk,q} - \xi_{lk,q})^2} \quad (58)$$

where Q is the number of experiments and ξ represents the azimuth angle or the elevation angle. The condition for judging the success of the estimation is that the sum of the RMSE of

TABLE V
SIMULATION PARAMETERS

Parameter	Value
NC-EMVA numbers, M_r , M_t	2
Number of antenna elements	12
IES (λ_c)	15
Carrier frequency (GHz)	28
Bandwidth (MHz)	500
Cluster number, L	2
Ray number in cluster l	14
FFT point, N_s	1024
Subsequence number, L_{seq}	300
Snapshot number, N	100

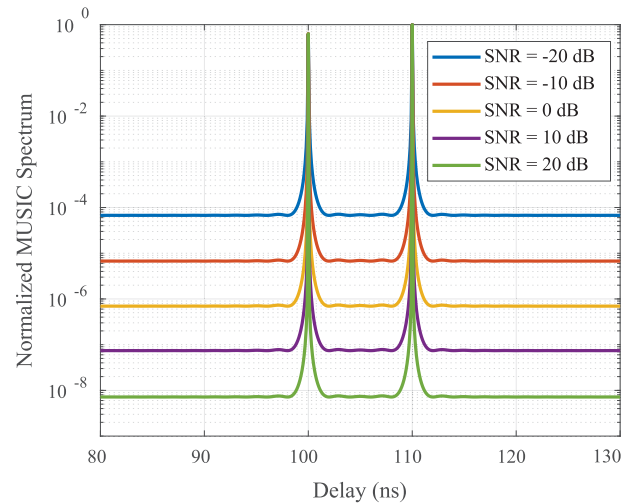


Fig. 7. The normalized MUSIC delay spectrum with different SNRs.

the azimuth angle and the elevation angle is less than 1 degree. The probability of success is obtained by the success times in 100 simulations.

A. Performance Comparison of Different Polarized Arrays

In Fig. 6, with different polarized antennas in the 6×6 MIMO system, the performance comparison of the probability of success is shown. The 6 antenna elements are arranged as a 3×2 rectangle array with $\text{IES} = 15\lambda_c$. There are 2 clusters with the number of rays in each cluster being 7. The subsequence number is 100. The rest parameters are given in Table V. It is found that the probability of success achieves 100% for both the uni-polarized array and the cross-polarized array at the SNR of about 9 dB. For the NC-EMVA, the required SNR is only about 6 dB. That is to say, the NC-EMVA has a better performance than uni-polarized and cross-polarized arrays. It is worthy to notice that the XPR cannot be estimated when using the uni-polarized array.

B. Simulation Setup

In this subsection, the setup of the simulations is given in detail in Table V. For the system configuration, the setup of the transmitting antenna array and receiving antenna array are the same, and both arrays are equipped with two EMVAs (12 antenna elements), respectively. The 12 antenna elements

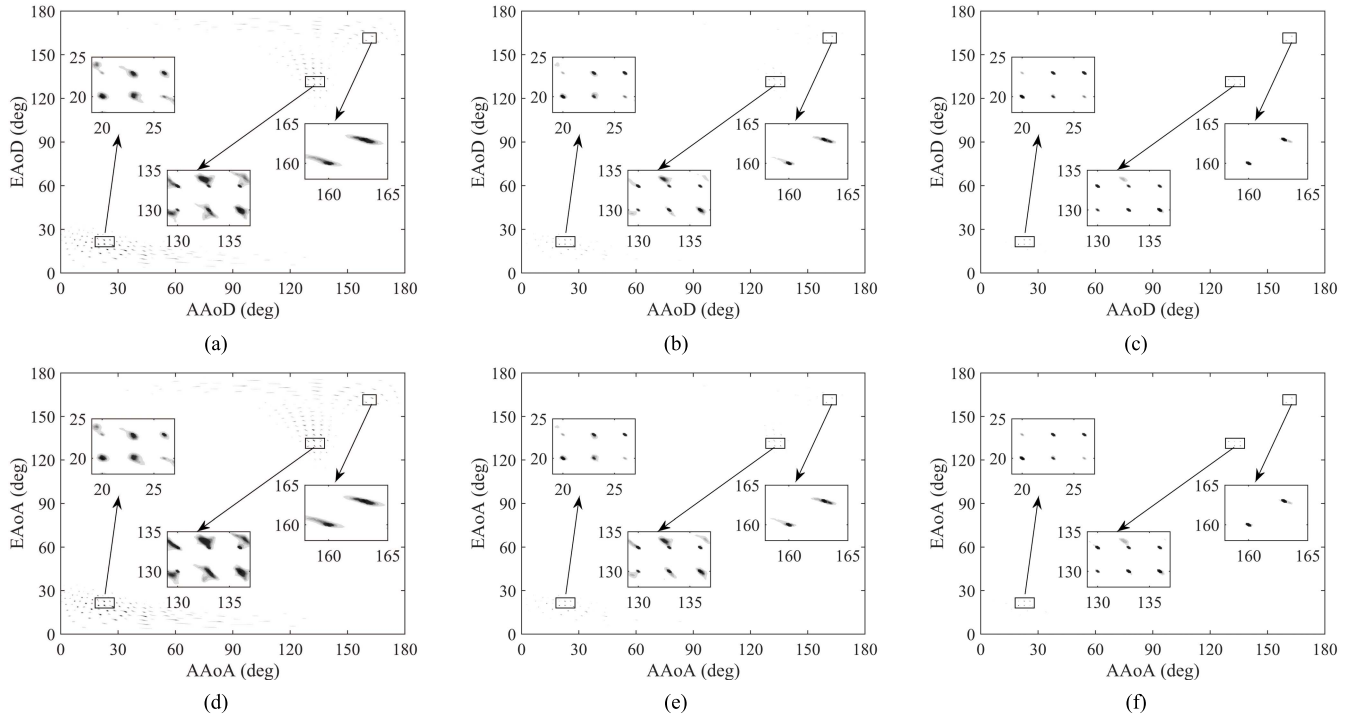


Fig. 8. The AoD and AoA MUSIC spectra with different SNRs: (a) AoD, SNR = 0 dB; (b) AoD, SNR = 5 dB; (c) AoD, SNR = 10 dB; (d) AoA, SNR = 0 dB; (e) AoA, SNR = 5 dB; (f) AoA, SNR = 10 dB.

are arranged as a rectangle array with size 3×4 . The carrier frequency is set to be 28 GHz, the IES is larger than half of the carrier wavelength, and the bandwidth of the signals is 500 MHz. To investigate the robustness and accuracy of the proposed method, three kinds of situations ($\text{IES} = 5\lambda_c, 10\lambda_c,$ and $15\lambda_c$) are considered where λ_c is the wavelength of the carrier frequency. The length of the subsequence is set to $N_s = 1024$, which is equal to the number of FFT points. The number of subsequences is set to $L_{\text{seq}} = 300$. In the frequency domain smoothing procedure, the number of virtual subarrays is set to $P = 8$. The number of snapshots is set to $N = 100$, which is larger than the number of rays.

Two clusters are generated in the simulation. The delays of the two clusters are set to $\tau = [100, 110]$ ns. Each cluster contains 14 rays. The number of rays is larger than the number of antenna array elements, which is 12 in the simulation. The EAoD and EAoA are set in the range of $[0^\circ, 180^\circ]$. The AAoD and AAoA are also set in the range of $[0^\circ, 180^\circ]$. The angles of some rays are set close to each other. These rays are usually scattered or reflected by the closely spaced scatters or reflectors in the propagation environment. The XPRs of all rays are set uniformly from 1 to K to cover the possible range for XPRs. The initial phases are set randomly from $-\pi$ to π . The amplitude of each ray is set to fluctuate around a fixed value for different snapshots. Some of the rays are set with larger amplitudes, and the rest are set with smaller amplitudes to show the estimation ability for the rays with different powers.

C. Parameter Estimation With Different SNRs

The normalized MUSIC delay spectrum under different SNRs is shown in Fig. 7. Delays can be accurately estimated

even under very low SNR conditions. The AoA and AoD estimations are based on the delay estimation results, so accurate delay estimation is essential. The AoD and AoA MUSIC spectra under different SNRs are given in Fig. 8. The rays in one cluster usually result from the same scatter or scatters with a nearby position. Therefore, the angles are distributed in a small scope. Furthermore, some of the rays in one cluster may have the same azimuth or elevation angle. In the simulation of Fig. 8, the azimuth and the elevation of some rays are concentrated within a small degree range. The angle range of the rays in one cluster is $[0^\circ, 180^\circ]$. The proposed method can be used to estimate the AoD and AoA accurately when the number of rays in one cluster is larger than the number of antenna elements, even if some of the rays have the same azimuths or elevations. As the SNR increases, the peaks of the rays become more clear. The angles can be estimated unambiguously when the space between two antenna elements is larger than half the carrier wavelength, which is different from traditional methods. The reason for the unambiguity of the angle estimation is that the virtual array elements are generated via a broadband array response.

Fig. 9 shows the probability of success for the AoD and AoA estimation. The IES is $15\lambda_c, 10\lambda_c,$ or $5\lambda_c$ and N_v is set to 12 or 128. It can be seen from the results that N_v will not have a big impact on the probability of success. This is because the frequency bins in the virtual subarray are of high redundancy for the steering matrix construction. Note that the reduction of N_v will lead to a decrease in estimation complexity. Therefore, the selection of the frequency bins should take the estimation complexity constraints and (56) into consideration in the practical implementation. For larger IES, the probability of success approaches 100% under a

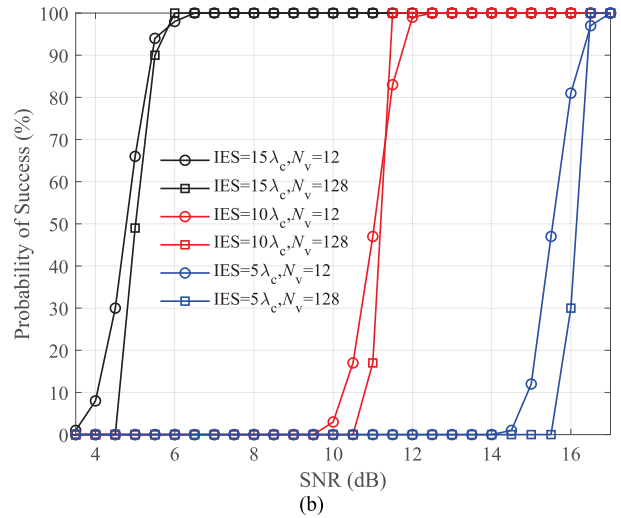
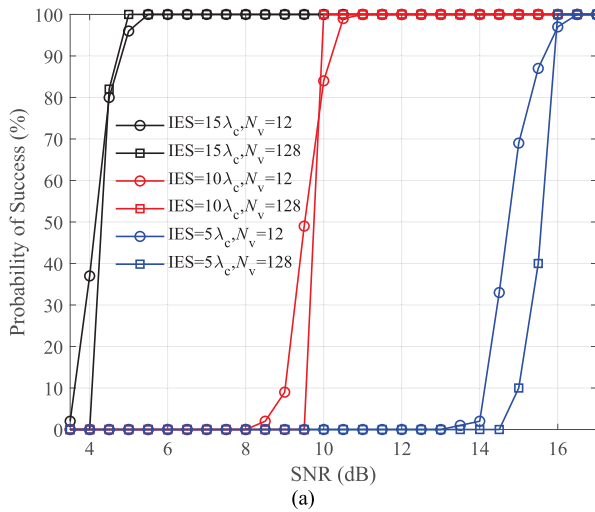


Fig. 9. The probability of success for AoD and AoA with different SNRs. (a) AoD; (b) AoA.

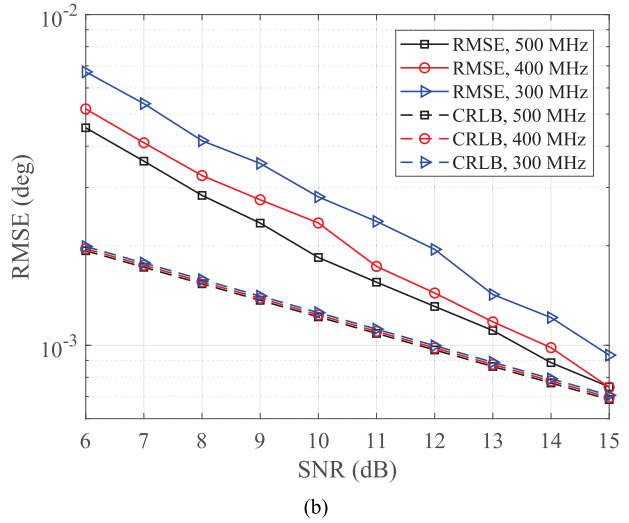
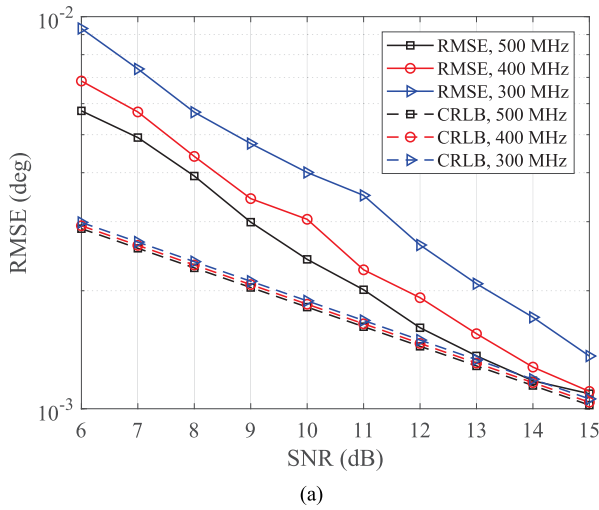


Fig. 10. The RMSE of AoD estimation under different SNRs with three different bandwidths. (a) AAoD; (b) EAoD.

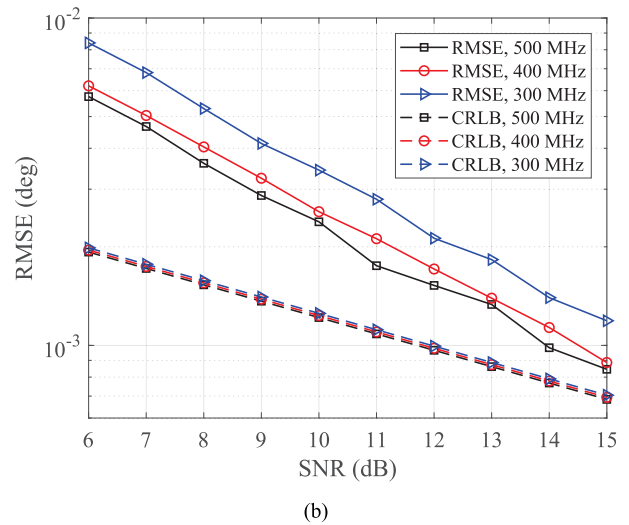
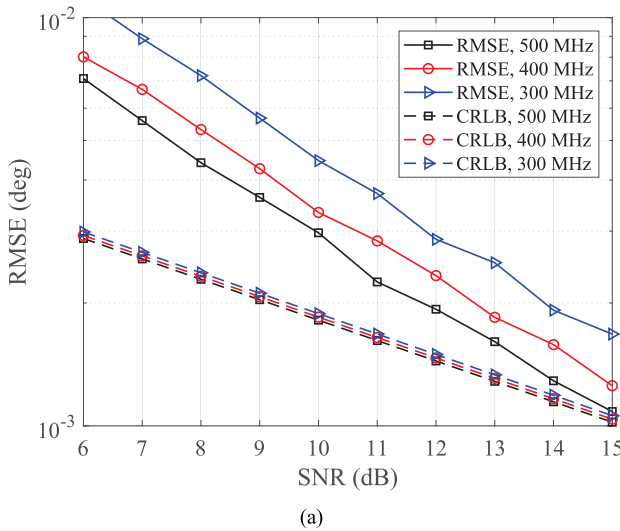


Fig. 11. The RMSE of AoA estimation under different SNRs with three different bandwidths. (a) AAoA; (b) EAoA.

lower SNR. This is because the array aperture increases with increasing IES under the same bandwidth.

Fig. 10 gives the RMSE of the estimated AAoD and EAoD with different bandwidths. Fig. 11 shows the RMSE of the

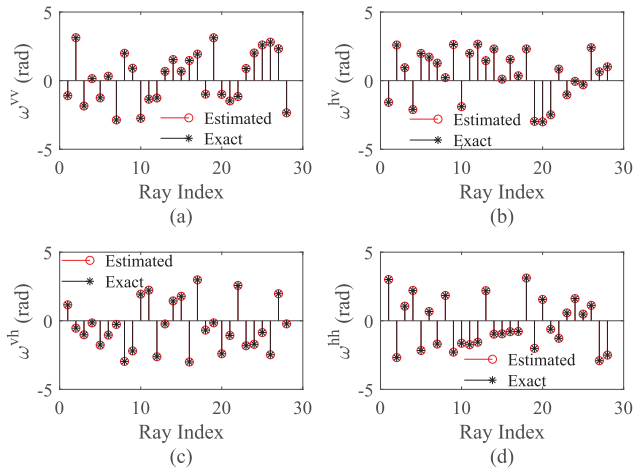


Fig. 12. The initial phases estimation results with SNR = 10 dB for (a) ω^{vv} , (b) ω^{hv} , (c) ω^{vh} , and (d) ω^{hh} .

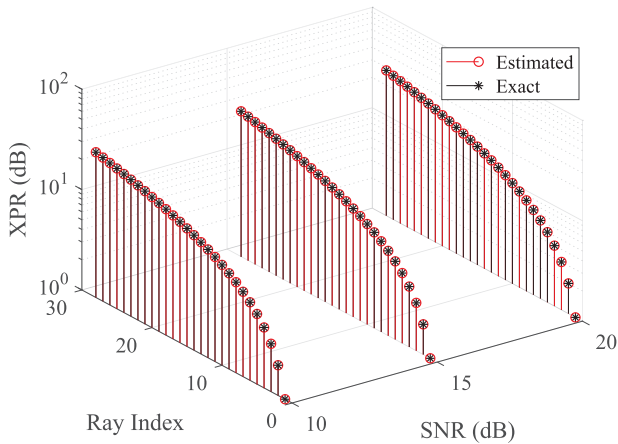


Fig. 13. The XPR estimation results under different SNRs.

estimated AAoA and EAoA with different bandwidths. Here, the N_v is set as 128. The results show that the RMSE is affected by the bandwidth. At the same SNR, a wider signal bandwidth leads to better RMSE performance. This is because the larger bandwidth will lead to a larger virtual array aperture. The experiments are performed one hundred times to reduce uncertainty. The CRLB of each situation is given for comparison. The simulation results show that the RMSEs of the proposed method are close to those of the CRLB as the SNR increases. The XPR estimation result of each ray in all clusters, given in Fig. 13, is accurately estimated. The exact value stands for the XPR set in the simulation. The estimated value stands for the XPR estimated by the proposed method. In the simulation, there are two clusters with 14 rays in each cluster. Fig. 12 gives the estimation results of the four initial phases under 10 dB SNR. The four initial phases are randomly generated in the range of $[-\pi, \pi]$. The exact value stands for the initial phases set in the simulations. As shown, the estimated value and the exact value of the four initial phases fit well for all of the rays under 10 dB SNR. Fig. 14 gives the estimation results of the amplitude of all the rays in N snapshots. In the simulation, most of the rays are set with weak power fluctuating in a small range, and only a few

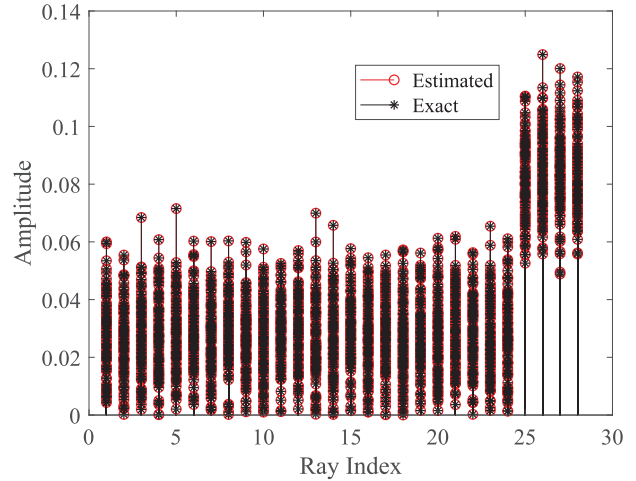


Fig. 14. The amplitude estimation results when SNR = 10 dB.

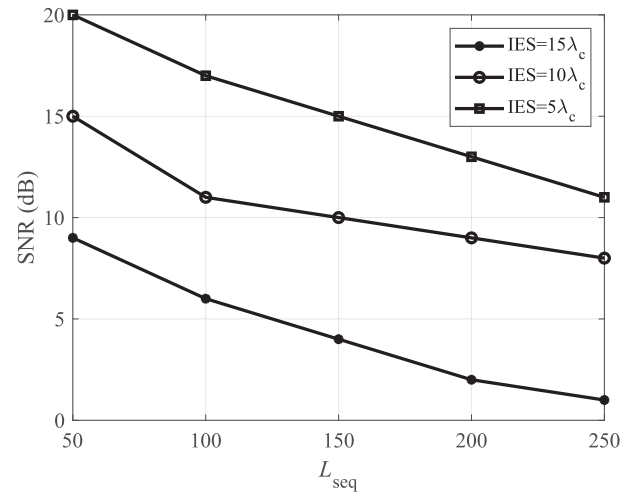


Fig. 15. The relationship between the minimum required SNR and L_{seq} with 100% probability of success.

rays are set with strong power. This situation setting is usually practical in a real radio propagation environment. The results show that the amplitude for all of the rays can be estimated accurately under a SNR of 10 dB.

The minimum SNR required to extract all the rays successfully under different L_{seq} with different array sizes is plotted in Fig. 15. The required minimum SNR decreases as L_{seq} and the array size increases because the increase in L_{seq} can suppress the influence of noise and the increase in the array size can enlarge the array aperture. The simulation results can be used to guide the design of a multipolarized channel measurement system that uses the proposed BEAR-based subspace estimation method.

V. CONCLUSION

A BEAR-based subspace estimation method has been proposed to estimate the delay, azimuth and elevation angles of arrival and departure, amplitude, XPR, and initial phase with EMVAA for multipolarized channel measurements. By extending the array response in the SFP domain, the proposed method can estimate a large number of rays in one cluster and is not limited by the number of antenna elements. The proposed

method works even if the rays have similar azimuths and elevations. The XPR, which is usually obtained coarsely based on the power ratio of each polarized antenna element, can be estimated accurately with the proposed method. In addition, the four initial phases of different polarization combinations are estimated accurately. The IES can be larger than half the carrier wavelength without angle ambiguity in the angle estimation. Thus, mutual coupling is effectively suppressed. Simulation results show that larger bandwidth leads to a smaller RMSE of the AoA and AoD. Moreover, larger IES leads to smaller required SNR. The proposed method holds promise for multiparameter estimation in future multipolarized channel measurements.

APPENDIX A DERIVATION OF THE RANK-DEFICIENT MUSIC SPECTRUM OF AOD

The steering matrix of the channel response matrix related to the transmitting antenna array and the reference receiving antenna element is $\tilde{\mathbf{B}}_t$, which is related to $\tilde{\mathbf{B}}_{f_i}$ as (38). According to (20) and (39), the column of $\tilde{\mathbf{B}}_{f_i}$ can be rewritten as $\tilde{\mathbf{b}}_{f_i, lk} = (\mathbf{A}_{t, f_i, lk} \otimes \boldsymbol{\rho}) \boldsymbol{\beta}_{lk}$.

$\boldsymbol{\rho}$ is a 1-by-2 vector, which represents the polarization component of the reference receiving antenna element. In this work, it is denoted by the first row of $\boldsymbol{\Omega}(\Theta_{r, lk})$. Let $\mathbf{A}_{t, lk}$ be

$$\mathbf{A}_{t, lk} = \left[e^{-j2\pi f_1 \tau_l} \mathbf{A}_{t, f_1, lk}^T, \dots, e^{-j2\pi f_{N_s} \tau_l} \mathbf{A}_{t, f_{N_s}, lk}^T \right]^T. \quad (59)$$

Then, the column of $\tilde{\mathbf{B}}_t$ can be written as $\tilde{\mathbf{b}}_{t, lk} = (\mathbf{A}_{t, lk} \otimes \boldsymbol{\rho}) \boldsymbol{\beta}_{lk}$.

In order to decrease the MUSIC searching dimension, the rank-deficient MUSIC technique is applied in AoD estimation [32]. Let $\mathbf{A}_{\text{AoD}, lk} = \mathbf{A}_{t, lk} \otimes \boldsymbol{\rho}$, the spectrum can be written as

$$P_t(\Theta_{t, lk}) = \det \left\{ \left| \mathbf{A}_{\text{AoD}, lk}^H(\Theta_{t, lk}) \mathbf{U}_{\text{tn}} \mathbf{U}_{\text{tn}}^H \mathbf{A}_{\text{AoD}, lk}(\Theta_{t, lk}) \right| \right\}. \quad (60)$$

Because the columns of $\mathbf{A}_{\text{AoD}, lk}$ depend linearly on $\mathbf{A}_{t, lk}$, (60) can be simplified as

$$P_t(\Theta_{t, lk}) = \det \left\{ \left| \mathbf{A}_{t, lk}^H(\Theta_{t, lk}) \mathbf{U}_{\text{tn}} \mathbf{U}_{\text{tn}}^H \mathbf{A}_{t, lk}(\Theta_{t, lk}) \right| \right\}. \quad (61)$$

APPENDIX B DERIVATION OF THE FREQUENCY DOMAIN SMOOTHING MUSIC SPECTRUM OF AOD AND AOA

Sort the N_v frequency bins in the subarray p as $[f_p, \dots, f_{\tilde{n}_v+p-1}, \dots, f_{N_s-P+p}]$, where \tilde{n}_v ranges from 1 to $N_s - P + 1$ and P is the number of virtual subarrays. Construct a selection matrix $\mathbf{J}_{f, p}$ with size N_v -by- N_s to select the frequency bins of the p th subarray. The n_v th row of $\mathbf{J}_{f, p}$ corresponds to the \tilde{n}_v th row of \mathbf{I}_{N_s} . Let us define a selection matrix for the p th subarray in the smoothing progress of AoD estimation $\mathbf{J}_{t, \text{sm}, p} = \mathbf{J}_{f, p} \otimes \mathbf{I}_{6M_t}$.

Let $\Phi_{t, p}$ be the phase-shifting matrix of adjacent frequency bins of the transmitting antenna elements, which can be

expressed as

$$\Phi_{t, p} = \begin{cases} \mathbf{1}_{6M_t N_v \times K}, & p = 0, \\ [\phi_{t, 11}, \dots, \phi_{t, 1K_1}, \dots, \phi_{t, L1}, \dots, \phi_{t, LK_L}], & p = 1, \\ \Phi_{t, p-1} \odot \Phi_{t, 1}, & p > 1, \end{cases} \quad (62)$$

where $\phi_{t, lk}$ is the column of $\Phi_{t, 1}$, and can be written as

$$\phi_{t, lk} = \left[e^{-j2\pi \Delta f (\tau_l + \frac{\mathbf{r}_{t, 1}^T \mathbf{u}_{t, lk}}{c})} \otimes \mathbf{1}_{1 \times N_v}, \dots, e^{-j2\pi \Delta f (\tau_l + \frac{\mathbf{r}_{t, 6M_t}^T \mathbf{u}_{t, lk}}{c})} \otimes \mathbf{1}_{1 \times N_v} \right]^T \quad (63)$$

with $\mathbf{r}_{t, i}$ being the coordinate of the i th transmitting element, $i = 1, \dots, 6M_t$ and Δf is the frequency interval of DFT. Then, let us reconstruct (37) as

$$\begin{aligned} \hat{\mathbf{H}}_{t, P} &= \frac{1}{P} \sum_{p=1}^P \mathbf{J}_{t, \text{sm}, p} \hat{\mathbf{H}}_t \\ &= \frac{1}{P} \tilde{\mathbf{B}}_{t, \text{sm}} \odot \boldsymbol{\Sigma}_t \boldsymbol{\Gamma} + \frac{1}{P} \sum_{p=1}^P \mathbf{J}_{t, \text{sm}, p} \mathbf{J}_t \mathbf{Z} \end{aligned} \quad (64)$$

where $\tilde{\mathbf{B}}_{t, \text{sm}} = \mathbf{J}_{t, \text{sm}, 1} \mathbf{J}_t \mathbf{B}$ and $\boldsymbol{\Sigma}_t = (\Phi_{t, 0} + \Phi_{t, 1} + \dots + \Phi_{t, P-1})$.

The covariance matrix of $\hat{\mathbf{H}}_{t, P}$ is

$$\mathbf{R}_{t, P} = \frac{1}{6M_t N_v} \hat{\mathbf{H}}_{t, P} \hat{\mathbf{H}}_{t, P}^H. \quad (65)$$

EVD of $\mathbf{R}_{t, P}$ leads to the $6M_t N_v \times (6M_t N_v - K)$ noise subspace $\mathbf{U}_{P\text{tn}}$. The smoothed AoD MUSIC spectrum can be expressed as

$$\bar{P}_t(\Theta_{t, lk}) = \det \left\{ \left| \bar{\mathbf{A}}_t^H(\Theta_{t, lk}) \mathbf{U}_{P\text{tn}} \mathbf{U}_{P\text{tn}}^H \bar{\mathbf{A}}_t(\Theta_{t, lk}) \right| \right\} \quad (66)$$

where the steering matrix $\bar{\mathbf{A}}_t(\Theta_{t, lk})$ is given as

$$\bar{\mathbf{A}}_t(\Theta_{t, lk}) = \mathbf{J}_{t, \text{sm}, 1} \mathbf{A}_t(\Theta_{t, lk}) \odot (\boldsymbol{\Sigma}_t \mathbf{e}_{lk} \otimes \mathbf{1}_{1 \times 2}). \quad (67)$$

APPENDIX C DERIVATION OF CRLB

Matrix Υ is the derivative of \mathbf{B} defined as $\Upsilon = \partial \mathbf{B} / \partial \boldsymbol{\vartheta} = [\partial \mathbf{b}_{11} / \partial \vartheta_{11} \dots \partial \mathbf{b}_{LK_L} / \partial \vartheta_{LK_L}]$, where $\boldsymbol{\vartheta}$ refers to the estimated parameter vector and \mathbf{b} is the column of \mathbf{B} given as

$$\mathbf{b}_{lk} = \left[e^{-j2\pi f_1 \tau_l} \mathbf{b}_{\text{tr} f_1, lk}^T, \dots, e^{-j2\pi f_{N_s} \tau_l} \mathbf{b}_{\text{tr} f_{N_s}, lk}^T \right]^T. \quad (68)$$

Note that the antenna pattern is discrete in the space domain and cannot be differentiated. Without loss of generality, it is regarded as a unit gain in the calculation progress. The details of the derivation process for the CRLB are similar to those of [30] and are not presented.

REFERENCES

- [1] T. S. Rappaport, G. R. MacCartney, M. K. Samimi, and S. Sun, "Wide-band millimeter-wave propagation measurements and channel models for future wireless communication system design," *IEEE Trans. Commun.*, vol. 63, no. 9, pp. 3029–3056, Sep. 2015.
- [2] C.-X. Wang, J. Bian, J. Sun, W. Zhang, and M. Zhang, "A survey of 5G channel measurements and models," *IEEE Commun. Surveys Tuts.*, vol. 20, no. 4, pp. 3142–3168, 4th Quart., 2018.
- [3] *Study on Channel Model for Frequencies From 0.5 to 100 GHz*, Standard TR 38.901 V15.0.0, 3GPP, 3rd Generation Partnership Project (3GPP), Tech. Rep., Jun. 2018.
- [4] *Study on Channel Model for Frequency Spectrum Above 6 GHz*, Standard TR 38.900 V15.0.0, Generation Partnership Project (3GPP), Tech. Rep., Jun. 2018.
- [5] J. Zhang, C. Pan, F. Pei, G. Liu, and X. Cheng, "Three-dimensional fading channel models: A survey of elevation angle research," *IEEE Commun. Mag.*, vol. 52, no. 6, pp. 218–226, Jun. 2014.
- [6] D. Piao and Y. Wang, "Experimental evaluation of the tri-polarized MIMO channel properties based on a compact multimode antenna," *IEEE Access*, vol. 7, pp. 67807–67817, 2019.
- [7] D. Piao, "Characteristics of the hexapolarized MIMO channel over free-space and three non-free-space scenarios," *IEEE Trans. Wireless Commun.*, vol. 12, no. 8, pp. 4174–4182, Aug. 2013.
- [8] M. R. Andrews, P. P. Mitra, and R. deCarvalho, "Tripling the capacity of wireless communications using electromagnetic polarization," *Nature*, vol. 409, no. 6818, pp. 316–318, Jan. 2001.
- [9] M.-T. Dao, V.-A. Nguyen, Y.-T. Im, S.-O. Park, and G. Yoon, "3D polarized channel modeling and performance comparison of MIMO antenna configurations with different polarizations," *IEEE Trans. Antennas Propag.*, vol. 59, no. 7, pp. 2672–2682, Jul. 2011.
- [10] Y. He, X. Cheng, and G. L. Stuber, "On polarization channel modeling," *IEEE Wireless Commun.*, vol. 23, no. 1, pp. 80–86, Feb. 2016.
- [11] M. Coldrey, "Modeling and capacity of polarized MIMO channels," in *Proc. VTC Spring IEEE Veh. Technol. Conf.*, May 2008, pp. 440–444.
- [12] A. S. Y. Poon and D. N. C. Tse, "Degree-of-freedom gain from using polarimetric antenna elements," *IEEE Trans. Inf. Theory*, vol. 57, no. 9, pp. 5695–5709, Sep. 2011.
- [13] X. Wang, L. Wan, M. Huang, C. Shen, and K. Zhang, "Polarization channel estimation for circular and non-circular signals in massive MIMO systems," *IEEE J. Sel. Topics Signal Process.*, vol. 13, no. 5, pp. 1001–1016, Sep. 2019.
- [14] A. Nehorai and E. Paldi, "Vector-sensor array processing for electromagnetic source localization," *IEEE Trans. Signal Process.*, vol. 42, no. 2, pp. 376–398, Feb. 1994.
- [15] K. T. Wong and M. D. Zoltowski, "Uni-vector-sensor ESPRIT for multistore azimuth, elevation, and polarization estimation," *IEEE Trans. Antennas Propag.*, vol. 45, no. 10, pp. 1467–1474, Oct. 1997.
- [16] J. Duploup, C. Morlaas, H. Aubert, P. Potier, and P. Pouliguen, "Wide-band vector antenna for dual-polarized and three-dimensional direction-finding applications," *IEEE Antennas Wireless Propag. Lett.*, vol. 18, no. 8, pp. 1572–1575, Aug. 2019.
- [17] K. T. Wong and X. Yuan, "Vector cross-product direction-finding with an electromagnetic vector-sensor of six orthogonally oriented but spatially noncollocating dipoles/loops," *IEEE Trans. Signal Process.*, vol. 59, no. 1, pp. 160–171, Jan. 2011.
- [18] X. Yuan, "Spatially spread dipole/loop quads/quints: For direction finding and polarization estimation," *IEEE Antennas Wireless Propag. Lett.*, vol. 12, pp. 1081–1084, 2013.
- [19] Y. Bresler and A. Macovski, "Exact maximum likelihood parameter estimation of superimposed exponential signals in noise," *IEEE Trans. Acoust., Speech, Signal Process.*, vol. 34, no. 5, pp. 1081–1089, Oct. 1986.
- [20] Y.-Y. Wang, J.-T. Chen, and W.-H. Fang, "TST-MUSIC for joint DOA-delay estimation," *IEEE Trans. Signal Process.*, vol. 49, no. 4, pp. 721–729, Apr. 2001.
- [21] M. C. Vanderveen, A.-J. Van Der Veen, and A. Paulraj, "Estimation of multipath parameters in wireless communications," *IEEE Trans. Signal Process.*, vol. 46, no. 3, pp. 682–690, Mar. 1998.
- [22] B. H. Fleury, M. Tschudin, R. Heddergott, D. Dahlhaus, and K. Ingeman Pedersen, "Channel parameter estimation in mobile radio environments using the SAGE algorithm," *IEEE J. Sel. Areas Commun.*, vol. 17, no. 3, pp. 434–450, Mar. 1999.
- [23] R. Zhang, S. Wang, X. Lu, W. Duan, and L. Cai, "Two-dimensional DoA estimation for multipath propagation characterization using the array response of PN-sequences," *IEEE Trans. Wireless Commun.*, vol. 15, no. 1, pp. 341–356, Jan. 2016.
- [24] G. G. Raleigh and T. Boros, "Joint space-time parameter estimation for wireless communication channels," *IEEE Trans. Signal Process.*, vol. 46, no. 5, pp. 1333–1343, May 1998.
- [25] X. Yin, L. Ouyang, and H. Wang, "Performance comparison of SAGE and MUSIC for channel estimation in direction-scan measurements," *IEEE Access*, vol. 4, pp. 1163–1174, 2016.
- [26] B. Yang, P. Zhang, H. Wang, and W. Hong, "Efficient delay and AoA estimation using vector antenna for radio propagation measurements," in *Proc. IEEE Int. Symp. Antennas Propag. USNC-URSI Radio Sci. Meeting*, Jul. 2019, pp. 2125–2126.
- [27] B. Yang, P. Zhang, H. Wang, and W. Hong, "Electromagnetic vector antenna array-based multi-dimensional parameter estimation for radio propagation measurement," *IEEE Wireless Commun. Lett.*, vol. 8, no. 6, pp. 1608–1611, Dec. 2019.
- [28] G. Zheng, "Two-dimensional DOA estimation for polarization sensitive array consisted of spatially spread crossed-dipole," *IEEE Sensors J.*, vol. 18, no. 12, pp. 5014–5023, Apr. 2018.
- [29] S. Khan and K. T. Wong, "A six-component vector sensor comprising electrically long dipoles and large loops—To simultaneously estimate incident sources' directions-of-arrival and polarizations," *IEEE Trans. Antennas Propag.*, vol. 68, no. 8, pp. 6355–6363, Aug. 2020.
- [30] P. Stoica and A. Nehorai, "MUSIC, maximum likelihood, and cramer-rao bound," *IEEE Trans. Acoust., Speech, Signal Process.*, vol. 37, no. 5, pp. 720–741, May 1989.
- [31] Y. Yan and M. Ma, "SNR improvement for energy detection of narrow band signal in OFDM system," *IEEE Commun. Lett.*, vol. 18, no. 11, pp. 1967–1970, Nov. 2014.
- [32] X. Zhang, C. Chen, J. Li, and D. Xu, "Blind DOA and polarization estimation for polarization-sensitive array using dimension reduction MUSIC," *Multidimensional Syst. Signal Process.*, vol. 25, no. 1, pp. 67–82, Jan. 2014.



Bensheng Yang (Graduate Student Member, IEEE) received the B.S. degree from Northeastern University at Qinhuangdao, Qinhuangdao, China, in 2013, and the M.S. degree from Xidian University, Xi'an, China, in 2016. He is currently pursuing the Ph.D. degree with the State Key Laboratory of Millimeter Waves, Southeast University, Nanjing, China. From 2016 to 2017, he was an Engineer with Huawei Technologies Company Ltd., Nanjing.

His current research interests include electromagnetic vector antenna design, radio propagation measurements, and signal processing.



Peize Zhang (Graduate Student Member, IEEE) received the B.S. degree (Hons.) in electrical engineering from the Beijing University of Posts and Telecommunications, Beijing, China, in 2015, and the M.S. degree (Hons.) in electrical engineering from the China Academy of Telecommunications Technology, Beijing, in 2018. He is currently pursuing the Ph.D. degree with the State Key Laboratory of Millimeter Waves, Southeast University, Nanjing, China.

His current research interests include millimeterwave radio propagation measurements, channel modeling, and millimeter-wave wireless network design.



Haiming Wang (Member, IEEE) was born in 1975. He received the B.S., M.S., and Ph.D. degrees in electrical engineering from Southeast University, Nanjing, China, in 1999, 2002, and 2009, respectively.

In 2002, he joined the School of Information Science and Engineering, Southeast University, where he is currently a Professor. He is also a part-time Professor with Purple Mountain Laboratories, Nanjing. He has authored or coauthored more than 50 technical publications in IEEE TRANSACTIONS ON ANTENNAS AND PROPAGATION and other peer-reviewed academic journals. He has authored or coauthored more than 70 patents and 52 patents have been granted. He was awarded for contributing to the development of IEEE 802.11aj by the IEEE Standards Association in July 2018. His current research interests include AI-powered antenna and radiofrequency technologies, AI-powered channel measurement and modeling technologies, and millimeter-wave and THz wireless communications.



Cheng-Xiang Wang (Fellow, IEEE) received the B.Sc. and M.Eng. degrees in communication and information systems from Shandong University, China, in 1997 and 2000, respectively, and the Ph.D. degree in wireless communications from Aalborg University, Denmark, in 2004.

He was a Research Assistant with the Hamburg University of Technology, Hamburg, Germany, from 2000 to 2001, a Visiting Researcher with Siemens AG Mobile Phones, Munich, Germany, in 2004, and a Research Fellow with the University of Agder, Grimstad, Norway, from 2001 to 2005. He has been with Heriot-Watt University, Edinburgh, U.K., since 2005, where he was promoted to a Professor in 2011. In 2018, he joined Southeast University, China, as a Professor. He is also a part-time Professor with Purple Mountain Laboratories, Nanjing, China. He has authored four books, three book chapters, and more than 410 articles in refereed journals and conference proceedings, including 24 highly cited articles. He has also delivered 22 invited keynote speeches/talks and 7 tutorials in international conferences. His current research interests include wireless channel measurements and modeling, 6G wireless communication networks, and applying artificial intelligence to wireless communication networks.

Dr. Wang is a member of the Academia Europaea (The Academy of Europe), a fellow of the IET, an IEEE Communications Society Distinguished Lecturer in 2019 and 2020, and a Highly-Cited Researcher recognized by Clarivate Analytics, from 2017 to 2020. He is currently an Executive Editorial Committee Member of IEEE TRANSACTIONS ON WIRELESS COMMUNICATIONS. He has served as a TPC member, TPC chair, and general chair for more than 80 international conferences. He received 12 Best Paper Awards from IEEE GLOBECOM 2010, IEEE ICCT 2011, ITST 2012, IEEE VTC 2013-Spring, IWCMC 2015, IWCMC 2016, IEEE/CIC ICC 2016, WPMC 2016, WOCC 2019, IWCMC 2020, and WCSP 2020. He has served as an editor for nine international journals, including IEEE TRANSACTIONS ON WIRELESS COMMUNICATIONS from 2007 to 2009, IEEE TRANSACTIONS ON VEHICULAR TECHNOLOGY from 2011 to 2017, and IEEE TRANSACTIONS ON COMMUNICATIONS from 2015 to 2017. He was a Guest Editor of IEEE JOURNAL ON SELECTED AREAS IN COMMUNICATIONS, Special Issue on Vehicular Communications and Networks (Lead Guest Editor), Special Issue on Spectrum and Energy Efficient Design of Wireless Communication Networks, and Special Issue on Airborne Communication Networks. He was also a Guest Editor of IEEE TRANSACTIONS ON BIG DATA, Special Issue on Wireless Big Data, and is a Guest Editor of IEEE TRANSACTIONS ON COGNITIVE COMMUNICATIONS AND NETWORKING, Special Issue on Intelligent Resource Management for 5G and Beyond.



Xiaohu You (Fellow, IEEE) was born in 1962. He received the M.S. and Ph.D. degrees in electrical engineering from Southeast University, Nanjing, China, in 1985 and 1988, respectively.

Since 1990, he has been with the National Mobile Communications Research Laboratory, Southeast University, where he is currently the Director and a Professor. From 1999 to 2002, he was the Principal Expert of the C3G Project, where he was responsible for organizing China's 3G Mobile Communications Research and Development Activities. From 2001 to 2006, he was the Principal Expert of the China National 863 Beyond 3G FuTURE Project. Since 2013, he has been the Principal Investigator of the China National 863 5G Project. He has contributed more than 100 IEEE journal articles and two books in the areas of adaptive signal processing, neural networks, and their applications to communication systems. His research interests include mobile communication systems and signal processing and its applications.

Dr. You was selected as an IEEE Fellow due to his contributions to development of mobile communications in China, in 2011. He was a recipient of the National First Class Invention Prize in 2011. He served as the General Chair for the IEEE Wireless Communications and Networking Conference (WCNC) 2013, the IEEE Vehicular Technology Conference (VTC) 2016 Spring, and the IEEE International Conference on Communications (ICC) 2019. He is currently the Secretary General of the FuTURE Forum and the Vice Chair of the China IMT-2020 Promotion Group and the China National Mega Project on New Generation Mobile Network.